

# Automatic Outlier Rectification via Optimal Transport

Jose Blanchet<sup>\*1</sup>, Jiajin Li<sup>†1</sup>, Markus Pelger<sup>‡1</sup>, Greg Zanotti<sup>§1</sup>

<sup>1</sup>Department of Management Science & Engineering, Stanford University

March 22, 2024

## Abstract

In this paper, we propose a novel conceptual framework to detect outliers using optimal transport with a concave cost function. Conventional outlier detection approaches typically use a two-stage procedure: first, outliers are detected and removed, and then estimation is performed on the cleaned data. However, this approach does not inform outlier removal with the estimation task, leaving room for improvement. To address this limitation, we propose an automatic outlier rectification mechanism that integrates rectification and estimation within a joint optimization framework. We take the first step to utilize an optimal transport distance with a concave cost function to construct a rectification set in the space of probability distributions. Then, we select the best distribution within the rectification set to perform the estimation task. Notably, the concave cost function we introduced in this paper is the key to making our estimator effectively identify the outlier during the optimization process. We discuss the fundamental differences between our estimator and optimal transport-based distributionally robust optimization estimator. Finally, we demonstrate the effectiveness and superiority of our approach over conventional approaches in extensive simulation and empirical analyses for mean estimation, least absolute regression, and the fitting of option implied volatility surfaces.

## 1 Introduction

Outlier removal has a long tradition in statistics, both in theory and practice. This is because it is common to have (for example, due to collection errors) data contamination or corruption. Directly applying a learning algorithm to corrupted data can, naturally, lead to undesirable out-of-sample performance. Our goal in this paper is to provide a single-step optimization mechanism based on optimal transport for automatically removing outliers.

The challenge of outlier removal has been documented for many years (literally centuries); see e.g. (Gergonne, 1821) and (Peirce, 1852). Yet, the outlier removal problem continues to interest practitioners and researchers alike due to the danger of distorted model estimation mentioned above. A natural family of approaches followed in the literature takes the form of “two-stage” methods, which involve an outlier removal step followed by an estimation step. Methods within this family range from rules of thumb, such as removing outliers beyond a particular threshold based on a robust measure of scale like the interquartile range (Tukey, 1977), to various model-based or parametric distributional assumption-based tests (Thompson, 1985). While

---

<sup>\*</sup>jose.blanchet@stanford.edu

<sup>†</sup>jiajinli@stanford.edu

<sup>‡</sup>mpelger@stanford.edu

<sup>§</sup>gzanotti@stanford.edu

the two-stage approach can be useful by separating the estimation task from the outlier removal objective, it is not without potential pitfalls. For example, an outlier detection step that relies on a specific fitted model may tend to overfit to a particular type of outliers, which can mask the effect of other outliers (Rousseeuw & Leroy, 1987). On the other hand, the outlier detection step may be overly conservative, not being informed by a particular downstream task at hand. This can lead to a significant reduction in the number of observations available for model fitting in the next step, resulting in a loss of statistical efficiency (He & Portnoy, 1992). Despite these challenges, two-stage procedures remain popular among practitioners

Robust statistics, pioneered by Box (1953); Tukey (1960); Huber (1964) and others such as Hampel (1968, 1971) offers alternative approaches for obtaining statistical estimators in the presence of outliers without removing them, particularly in parametric estimation problems such as linear regression. Beyond these, one closely related approach is the minimum distance functionals-based estimator, introduced by Parr & Schucany (1980); Millar (1981); Donoho & Liu (1988a,b); Park et al. (1995); Zhu et al. (2022); Jaenada et al. (2022). This method involves projecting the corrupted distribution onto a family of distributions using a distribution discrepancy/metric and selecting the optimal estimator for the resulting distribution. It is important to note that this projection mechanism is not informed by the estimation task (such as fitting a linear regression or neural network). Thus, without additional information about the contamination model or the estimation task, it can be challenging to choose an appropriate family of distributions for the projection step, which may lead to similar limitations as those outlined earlier in practice.

In this paper, we propose a novel approach to integrate both outlier detection and estimation in a joint optimization framework. A key observation is that statisticians aim to “clean” data **before** decisions are made; thus, ideal robust statistical estimators tend to be optimistic. To address this, we introduce the rectification set—a ball centered around the empirical (contaminated) distribution and defined by the optimal transport distance (see (Villani, 2009; Peyré et al., 2019)) in probability space. This rectification set aims to exclude potential outliers and capture the true underlying distribution, allowing us to minimize the expectation over the “best-case” scenarios, leading to a min-min-type formulation. The study in Jiang & Xie (2024) also explores the connections with min-min type problems, which concentrates on the construction of some artificially constructed rectification sets to cover certain existing statistical estimators from the robust statistics literature. However, our primary focus is on introducing a novel rectification set, which is based on the optimal transport approach with a concave cost function.

To automatically detect outliers during the estimation process, one of our main contributions is the use of a concave cost function for the optimal transport distance. This function encourages “long hauls” transportation, in which the optimal transport plan moves only a portion of the data to a distant location, while leaving other parts unchanged. This strategic approach effectively repositions identified outliers closer to positions that better align with the clean data. Our novel formulation then involves minimizing the expected loss under the optimally rectified empirical distribution. This rectification is executed through the application of an optimal transport distance with a concave cost function, thereby correcting outliers to enhance performance within a fixed estimation task.

More importantly, our method distinguishes itself from distributionally robust optimization (DRO) (Bental et al., 2013; Bayraksan & Love, 2015; Wiesemann et al., 2014; Delage & Ye, 2010; Gao & Kleywegt, 2022; Blanchet & Kang, 2017; Shafieezadeh Abadeh et al., 2015; Shafieezadeh-Abadeh et al., 2019; Sinha et al., 2018; Kuhn et al., 2019) due to the distinctive correction mechanisms initiated by the robust formulation employing a min-min strategy.

As we discuss in Section 2 below, the timing of error generating differs crucially between DRO and robust statistics. DRO approach employs a min-max game strategy to control the worst-case loss over potential post-decision distributional shifts. In contrast, the robust estimator acts after the pre-decision distributional

contamination materializes. Thus the approach of robust statistics can be motivated as being closer to a max-min game against nature. As a consequence, in robust statistics, the adversary moves first, and therefore the statistician can be more optimistic that they can rectify the contamination applied by the nature thus motivating the min-min strategy suggested above.

We summarize our main contributions as follows:

- (i) **(Novel statistically robust estimator)** We propose a new statistically robust estimator that incorporates a novel rectification set constructed using the optimal transport distance. By employing a concave cost function within the optimal transport distance, our estimator enables automatic outlier rectification. We prove that the optimal rectified distribution can be found via a finite convex program and provide a cross-validation procedure for determining the optimal uncertainty region for determining the rectification set.
- (ii) **(Connection to adaptive quantile regression)** For mean estimation and least absolute regression, we demonstrate that the statistically robust estimator is equivalent to an adaptive quantile (regression) estimator, with the quantile controlled by the budget parameter  $\delta$ . Furthermore, we prove that the optimal rectified distribution exhibits a long-haul structure that facilitates outlier detection.
- (iii) **(Effectiveness in smoothing the implied volatility surface of real options)** We evaluate the performance of our estimator on various tasks, including mean estimation, least absolute regression, and a real-world application involving options implied volatility surface smoothing. Our experimental results demonstrate that our estimator produces surfaces that are 30.4% smoother compared to baseline estimators, indicating success in outlier removal because the curves should be smooth based on structural financial properties. Additionally, it achieves an average reduction of 6.3% in mean average percent error (MAPE) across all estimated surfaces, providing empirical evidence of the effectiveness of our rectifying optimal transporter.

## 2 DRO and Robust Statistics as Adversarial Games

In this section, we summarize conceptually how robust statistics are different with DRO, see [Blanchet et al. \(2024\)](#) for details. To lay a solid mathematical foundation, we begin by investigating a generic stochastic optimization problem. Here, we assume that  $Z$  is a random vector in space  $\mathcal{Z} \subseteq \mathbb{R}^d$  that follows the distribution  $\mathbb{P}_*$ . The set of feasible model parameters is denoted  $\Theta$  (assumed to be finite-dimensional to simplify). Given a realization  $z$  and a model parameter  $\theta \in \Theta$  the corresponding loss is  $\ell(\theta, z)$ . A standard expected loss minimization decision rule is obtained by solving

$$\min_{\theta \in \Theta} \mathbb{E}_{\mathbb{P}_*}[\ell(\theta, \xi)] = \int_{\Xi} \ell(\theta, \xi) d\mathbb{P}_*(\xi). \quad (2.1)$$

Since  $\mathbb{P}_*$  is generally unknown, to approximate the objective function in (2.1), we often gather  $n$  independent and identically distributed (i.i.d.) samples  $\{z_i\}_{i=1}^n$  from the unknown data-generating distribution  $\mathbb{P}_*$  and consider the empirical risk minimization counterpart,

$$\min_{\theta \in \Theta} \mathbb{E}_{\hat{\mathbb{P}}_n}[\ell(\theta, Z)] = \frac{1}{n} \sum_{i=1}^n \ell(\theta, z_i), \quad (2.2)$$

where  $\hat{\mathbb{P}}_n$  denotes the empirical measure  $\frac{1}{n} \sum_{i=1}^n \delta_{z_i}$  and  $\delta_z$  is the Dirac measure centered at  $z$ .

Then, we proceed to naturally introduce the general data-driven decision-making cycle as below:

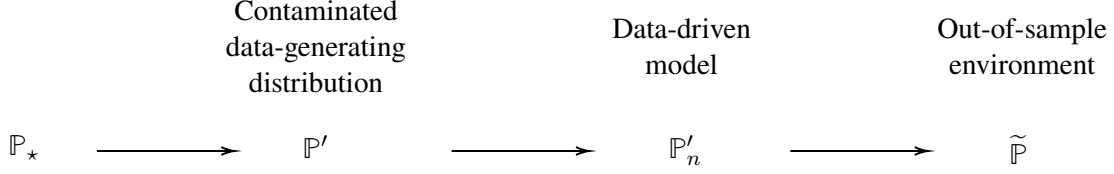


Figure 1: Data-Driven Decision Making Cycle

In the general data-driven decision-making cycle depicted in Figure 1, we usually collect  $n$  i.i.d samples from the unknown data-generating distribution  $\mathbb{P}'$ , which may be identical to or distinct from the clean distribution  $\mathbb{P}_*$ . Subsequently, we make a decision (e.g., parameter estimation) based on a model,  $\mathbb{P}'_n$ , built from these samples. Such a model could be parametric or non-parametric. These decisions are then put into action within the out-of-sample environment  $\tilde{\mathbb{P}}$ , which may or may not conform to the distribution  $\mathbb{P}_*$ . In this general cycle, the sample average method (2.1) may lead to poor out-of-sample guarantees.

Then, we aim to distinguish between DRO and robust statistics by treating them as adversarial games. The crucial distinction lies in the **timing** of contamination or attacks.

(i) (**DRO**:  $\tilde{\mathbb{P}} \neq \mathbb{P}_* = \mathbb{P}'$ ) The attack occurs in the **post-decision** stage. In this scenario, the out-of-sample environment  $\tilde{\mathbb{P}}$  diverges from the data-generating distribution  $\mathbb{P}_*$ , and no contamination occurs before the decision, implying that  $\mathbb{P}_* = \mathbb{P}'$ . For instance, in adversarial deployment scenarios, malicious actors can deliberately manipulate the data distribution to compromise the performance of trained models. With full access to our trained machine learning model, the adversary endeavors to create adversarial examples specifically designed to provoke errors in the model's predictions.

To ensure good performance in terms of the optimal expected population loss over the out-of-sample distribution, the DRO framework introduces an uncertainty set  $\mathcal{B}(\mathbb{P}'_n)$  to encompass discrepancies between the in-of-sample-distribution  $\mathbb{P}'_n$  and the out-of-sample distribution  $\tilde{\mathbb{P}}$ . Subsequently, the DRO formulation minimizes the worst-case loss within this uncertainty set, thereby aiming to:

$$\min_{\theta \in \Theta} \sup_{\mathbb{Q} \in \mathcal{B}(\mathbb{P}'_n)} \mathbb{E}_{\mathbb{Q}}[\ell(\theta, Z)]. \quad (2.3)$$

(ii) (**Robust Statistics**:  $\tilde{\mathbb{P}} = \mathbb{P}_* \neq \mathbb{P}'$ ) The contamination occurs in the **pre-decision** stage. Many real-world datasets exhibit outliers or measurement errors at various stages of data generation and collection. In such scenarios, the observed samples are generated by a contaminated distribution  $\mathbb{P}'$ , which differs from the underlying uncontaminated distribution  $\mathbb{P}_*$ . But, the out-of-sample distribution equals to the original clean distribution. In contrast with DRO, the adversary introduces worst-case corruption according to a certain contamination model to the clean data prior to the training of any machine learning models. Our objective is to clean the data during the training phase to achieve a robust classifier. It is noteworthy that the attacker does not have access to the specific model to be selected by the learner.

Given that the statistician knows that the data has been contaminated, a natural policy class to consider involves rectifying/correcting the contamination, and, for this, we introduce a rectification set  $\mathcal{R}(\mathbb{P}'_n)$  which models a set of possible pre-contamination distributions based on the knowledge of the empirical measure  $\mathbb{P}'_n$ . To ensure good performance in terms of the optimal expected population loss over the clean distribution, the rectification/decontamination approach naturally induces the following min-min strategy:

$$\min_{\theta \in \Theta} \min_{\mathbb{Q} \in \mathcal{R}(\mathbb{P}'_n)} \mathbb{E}_{\mathbb{Q}}[\ell(\theta, Z)]. \quad (2.4)$$

Again, our goal in this paper is in connection to (2.4) and thus completely different from DRO.

### 3 Automatic Outlier Rectification Mechanism

In this section, we introduce our primary contribution by delineating (2.4). Our estimator is crafted to incorporate outlier rectification and parameter estimation within a unified optimization framework, facilitating automatic outlier rectification.

A natural question arises from (2.4): how do we construct the rectification set in the space of probability distributions to correct the observed data set? In this paper, we employ an optimal transport distance to create a ball centered at the contaminated empirical distribution  $\mathbb{P}'_n$ .

**Definition 3.1** (Rectification Set). The optimal transport-based rectification set is defined as

$$\mathcal{R}(\mathbb{P}'_n) = \{\mathbb{Q} \in \mathcal{P}(\mathcal{Z}) : \text{ID}_c(\mathbb{Q}, \mathbb{P}'_n) \leq \delta\}, \quad (3.1)$$

where  $\delta > 0$  represents a radius, and  $\text{ID}_c$  is a specific optimal transport distance defined in Definition 3.2.  $\square$

**Definition 3.2.** (Optimal Transport Distance (Peyré et al., 2019; Villani, 2009)) Suppose that  $c(\cdot, \cdot) : \mathcal{Z} \times \mathcal{Z} \rightarrow [0, \infty]$  is a lower semi-continuous cost function such that  $c(z, z') = 0$  for all  $z, z' \in \mathcal{Z}$  satisfying  $z = z'$ . The optimal transport distance between two probability measures  $\mathbb{P}, \mathbb{Q} \in \mathcal{P}(\mathcal{Z})$  is defined as

$$\text{ID}_c(\mathbb{P}, \mathbb{Q}) = \inf_{\pi \in \mathcal{P}(\mathcal{Z} \times \mathcal{Z})} \left\{ \mathbb{E}_\pi[c(Z, Z')] : \pi_Z = \mathbb{P}, \pi_{Z'} = \mathbb{Q} \right\}.$$

Here,  $\mathcal{P}(\mathcal{Z} \times \mathcal{Z})$  is the set of joint probability distribution  $\pi$  of  $(Z, Z')$  supported on  $\mathcal{Z} \times \mathcal{Z}$  while  $\pi_Z$  and  $\pi_{Z'}$  respectively refer to the marginals of  $Z$  and  $Z'$  under the joint distribution  $\pi$ .  $\square$

If we consider  $c(z, z') = \|z - z'\|^r$  as a metric defined on  $\mathbb{R}^d$ , where  $r \in [1, \infty)$ , then the distance metric  $\text{ID}_c^{1/r}(\mathbb{P}, \mathbb{Q})$  corresponds to the  $r$ -th order Wasserstein distance (Villani, 2009). In this paper, we pioneer the utilization of *concave* cost functions, exemplified by  $c(z, z') = \|z - z'\|^r$  where  $r \in (0, 1)$  in statistical robust estimation. We note that  $\text{ID}_c(\mathbb{P}, \mathbb{Q})$  (as opposed to  $\text{ID}_c^{1/r}(\mathbb{P}, \mathbb{Q})$ ) is also a metric for  $r \in [0, 1)$ . The rationale behind selecting a concave cost function is intuitive: it promotes *long hauls* transportation plans, enabling outliers to be automatically moved significant distances back towards the central tendency of data distribution. This, in turn, facilitates automatic outlier rectification. Concave costs promote long hauls due to their characteristic of exhibiting decreasing marginal increases in transportation cost. In other words, if an adversary decides to transport a data point by  $\|\Delta\|$  units, it becomes cheaper to continue transporting the same point by an additional  $\epsilon$  distance compared to moving another point from its initial location.

**Remark 3.1.** (i) When we disregard the outer minimization concerning estimation parameters, the inner minimization problem over probability measures is closely linked to the minimum distance functionals-based estimator, initially proposed by (Donoho & Liu, 1988a). The estimator, is obtained by first projecting the corrupted distribution  $\mathbb{P}'_n$  onto a family of distributions  $\mathcal{G}$  under a certain distribution discrepancy measure  $\text{ID}$ . Then, the optimal parameters are selected for the resulting distribution. However, even with additional information about our contamination models, this “two-stage” procedure has two major drawbacks: the difficulty in choosing an appropriate family of distributions  $\mathcal{G}$  and the inherent computational challenge to project probability distributions. Moreover, the first stage (projection) is usually sensitive to the choice of family  $\mathcal{G}$ . In contrast, we propose a novel approach that integrates outlier rectification (i.e., explicit projection) and parameter estimation into a joint optimization framework in (2.4). (ii) This min-min strategy has also been explored in Jiang & Xie (2024) using an artificially constructed rectification set. Their primary focus is to utilize the min-min formulation to recover well-studied robust statistics estimators. In contrast, our focus is on a new conceptual framework for formulating novel estimators which have not been studied before.  $\square$

**Illustrative Example.** Next, we aim to provide empirical evidence showcasing the potency and efficacy of the concave cost function on a toy example.

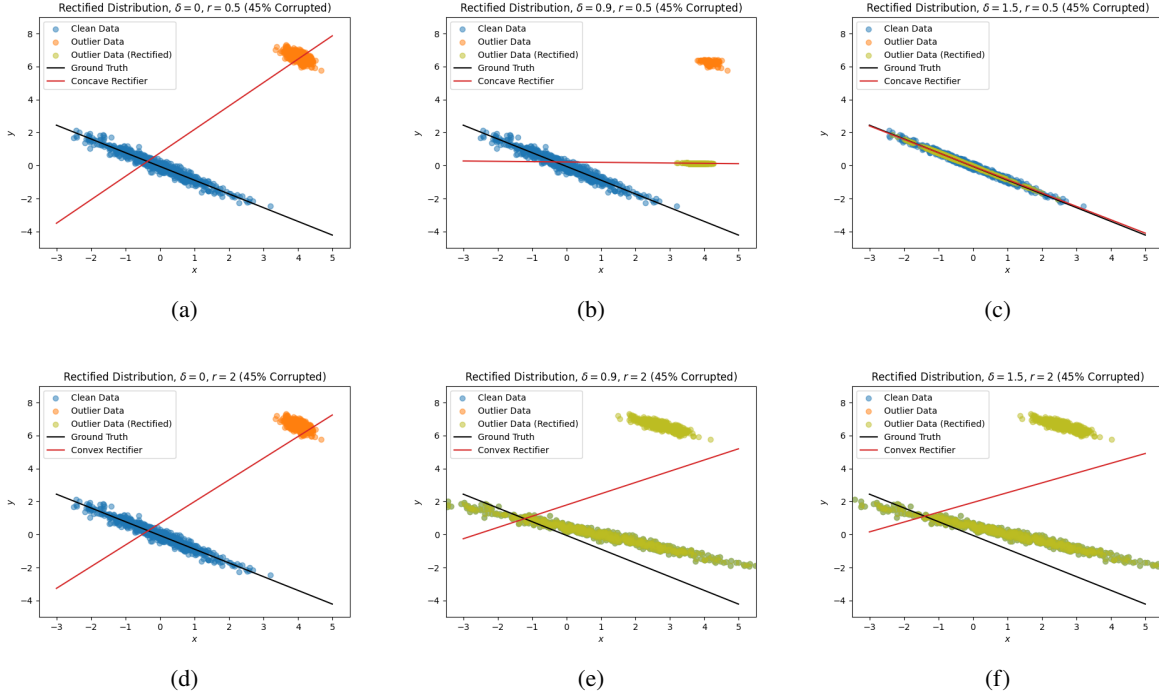


Figure 2: Visualization of contamination model: 55% are drawn with  $x \sim \mathcal{N}(0, 2)$  and  $y = 0.1 - 0.8x + 0.2w$ . 45% are drawn with  $x \sim \mathcal{N}(4, 2)$  and  $y = 10.1 - 0.8x + 0.2w$ . (a)-(c): In each case  $w \sim \mathcal{N}(0, 1)$ ; The rectified data generated by the proposed statistically robust estimator with different budget  $\delta$  and **concave** cost function (i.e.,  $r = 0.5$ ). (d)-(f): The rectified data generated by the proposed statistically robust estimator with different budget  $\delta$  and **convex** cost function (i.e.,  $r = 2$ ).

In this example, we perform linear regression using our estimator with either a concave or a convex transport cost function. The estimation is performed on a sample of points in  $\mathbb{R}^2$  drawn from a contaminated distribution (corresponding to  $\mathbb{P}'$ ) where 45% of the points are distributed according to an outlier distribution and 55% of the points are distributed according to the true uncontaminated distribution (corresponding to  $\mathbb{P}_*$ ). Our goal is to recover the line of best fit which corresponds to the uncontaminated distribution, which is  $y = 0.1 - 0.8x$ . We illustrate the considerable differences which can occur when using each of these cost functions under various choices of  $\delta$ , the rectification budget parameter. We depict this example in Figure 2.

The behavior of the estimator using the concave cost function is depicted in Figures 2(a)-(c). Each of these subfigures shows the points drawn from each distribution, the rectified distribution, the true line of best fit for the uncontaminated distribution, and the line of best fit produced by our estimator, at various choices of  $\delta$ . In Figure 2(a),  $\delta = 0$ , in Figure 2(b),  $\delta = 0.9$ , and in Figure 2(c),  $\delta = 1.5$ . As can be seen from the figures, as the budget  $\delta$  increases, we note that the proposed estimator using the concave cost function becomes increasingly adept at mitigating the influence of outlier data. It achieves this by rectifying the outlying points, moving them into the bulk of the uncontaminated distribution. As a result, the line of best fit (depicted in red) aligns much more closely with the true line of best fit (depicted in black). It is able to perform this successful estimation because each outlier point can be moved far with a cheap cost (a “long haul”) due to the use of the concave transport cost function.



However, the convex cost function may result in suboptimal estimators, which can only move every data point (clean and contaminated) a little bit. Figures 2(d)-(f) display the behavior of the estimator using the convex cost function, which illustrates this effect. Each subfigure displays the rectified distribution as yellow-green points for a different setting of  $\delta$  (i.e. (d)  $\delta = 0$ , (e)  $\delta = 0.9$ , and (f)  $\delta = 1.5$ ). As can be seen from the evolution of the rectified distribution, as  $\delta$  increases, instead of the outlier points being moved towards the bulk of the distribution, all of the points move towards each other—even the points in the clean distribution. This is not ideal behavior, as the points from the clean distribution should stay in place. This defective behavior causes the line of best fit produced by the estimator using the convex cost function (which is depicted in red) fit to the rectified points to be severely affected by the outliers; instead of being close to the ground truth line of best fit (which is depicted in black), its slope is moved significantly upwards towards the outliers. This occurs because the convex cost function gives lower cost to smaller rectifications of the given data set, which is an inappropriate assumption for data sets containing outliers.

Appendices C.5 and C.6 depict the evolution of the rectified distribution as  $\delta$  increases for the concave and convex cost functions, respectively. For our estimator which uses the concave cost, the evolution of the rectified distribution as  $\delta$  increases shows that our estimator increasingly rectifies the points in order of their distance from the line of best fit in a predictable and stable way. In contrast, the convex estimator consistently moves all points (clean and corrupted) toward each other as  $\delta$  changes, which achieves a poor estimate of the true line of best fit for all  $\delta$  considered.

## 4 Reformulation Results

With this intuition in hand, we focus on the derivation of equivalent reformulations for the infinite-dimensional optimization problem over probability measures in (2.4). These reformulations provide us with a fresh perspective on adaptive quantile regression or estimation, where the introduction of an efficient transporter rectifies the empirical distribution, effectively eliminating the influence of outliers.

To begin with, we can transform problem (2.4) into an equivalent finite-dimensional problem by leveraging the following strong duality theorem.

**Proposition 4.1** (Strong Duality). Suppose that  $\ell(\theta, \cdot)$  is lower semicontinuous and integrable under  $\mathbb{P}'_n$  for any  $\theta \in \Theta$ . Then, the strong duality holds, i.e.,

$$\inf_{Q \in \mathcal{R}(\mathbb{P}'_n)} \mathbb{E}_Q[\ell(\theta; Z)] = \max_{\lambda \geq 0} \mathbb{E}_{\mathbb{P}'_n} \left[ \min_{z \in \mathcal{Z}} \ell(\theta; Z') + \lambda c(z, Z') \right] - \lambda \delta.$$

□

The proof is essentially based on the strong duality results developed for Wasserstein distributionally robust optimization problems (Zhang et al., 2022; Li et al., 2022; Blanchet & Murthy, 2019; Gao & Kleywegt, 2022; Mohajerin Esfahani & Kuhn, 2018), which allows us to rewrite the original problem (2.4) as  $\inf_{Q \in \mathcal{R}(\mathbb{P}'_n)} \mathbb{E}_Q[\ell(\theta; Z)] = -\sup_{Q \in \mathcal{R}(\mathbb{P}'_n)} \mathbb{E}_Q[-\ell(\theta; Z)]$ .

We proceed to examine several representative examples to better understand the proposed statistically robust estimator (2.4). We begin with mean estimation to showcase our estimator's performance on one of the most classic problems of point estimation which can be easily understood. We then give an example for least absolute deviations (LAD) regression, one of the most important problems of robust statistics. LAD regression builds a conceptual foundation which leads into a discussion of our framework in more general cases and problem domains.

## 4.1 Mean Estimation

The mean estimation task is widely recognized as a fundamental problem in robust statistics, making it an essential example to consider. In this context, we define the loss function as  $\ell(\theta; z) = \|\theta - z\|$ . It is worth noting that when  $\delta = 0$ , Problem (2.4) is equivalent to the median, which has already been proven effective in the existing literature. However, beyond the equivalence to the median, there are additional benefits to be explored regarding the proposed rectification set. By deriving the equivalent reformulation and analyzing the optimal rectified distribution, we can gain further insights into how the proposed statistically robust estimator operates. This analysis provides valuable intuition into the workings of the estimator and its advantages.

**Theorem 4.1** (Mean Estimation). Suppose that  $\mathcal{Z} = \mathbb{R}^d$ ,  $\ell(\theta; z) = \|\theta - z\|$  and the cost function is defined as  $c(z, z') = \|z - z'\|^r$  where  $r \in (0, 1)$ . Without loss of generality, suppose that the following condition holds

$$\|\theta - z'_1\| \leq \|\theta - z'_2\| \leq \dots \leq \|\theta - z'_n\|. \quad (4.1)$$

Then, we have

$$\min_{Q \in \mathcal{R}(\mathbb{P}'_n)} \mathbb{E}_Q[\|\theta - Z\|] = \max \left( \frac{1}{n} \sum_{i=1}^{k(\theta)-1} \|\theta - z'_i\| + \frac{1}{n} \left( 1 - \frac{n\delta - \sum_{i=k(\theta)+1}^n \|\theta - z'_i\|^r}{\|\theta - z'_{k(\theta)}\|^r} \right) \|\theta - z'_{k(\theta)}\|, 0 \right). \quad (4.2)$$

where  $k(\theta) := \max_{k \in [n]} \left\{ k : \frac{1}{n} \sum_{i=k}^n \|\theta - z'_i\|^r \geq \delta \right\}$ .  $\square$

**Remark 4.1.** The resulting reformulation problem can be viewed as finding a quantile of  $\|\theta - z'\|$  controlled by the budget  $\delta$ . If we have a sufficient budget  $\delta$  such that  $\mathbb{E}_{\mathbb{P}'_n}[\|\theta - Z'\|^r] \leq \delta$ , it implies that all data points have been rectified to the value of  $\theta$ . Consequently, the minimum value of  $\min_{Q \in \mathcal{R}(\mathbb{P}'_n)} \mathbb{E}_Q[\ell(\theta, Z)]$  will be equal to zero. In non-trivial cases, when given a budget  $\delta > 0$  and the current estimator  $\theta$ , our objective is to identify and rectify the outliers in the observed data. To achieve this, we begin by sorting the data points based on their loss value  $\|\theta - z'_i\|$ . We relocate the data points starting with the one having the largest loss value,  $z'_n$ . The goal is to move each data point towards the current mean estimation  $\theta$  until the entire budget is fully utilized.  $\square$

*Proof.* Before we prove the theorem, it is worth highlighting that for any fixed  $\theta$ , we can always sort  $\{z_i\}_{i=1}^n$  based on the error  $\|\theta - z'_i\|$  to satisfy the condition (4.1).

By the strong duality result in Proposition 4.1, we have

$$\begin{aligned} \min_{Q \in \mathcal{B}(\mathbb{P}'_n)} \mathbb{E}_Q[\|\theta - Z'\|] &= \max_{\lambda \geq 0} \mathbb{E}_{\mathbb{P}'_n} \left[ \min_{\Delta \in \mathbb{R}} \|\theta - Z' - \Delta\| + \lambda \|\Delta\|^r \right] - \lambda \delta \\ &= \max_{\lambda \geq 0} \mathbb{E}_{\mathbb{P}'_n} \left[ \min_{0 \leq \|\Delta\| \leq \|\theta - Z'\|} \|\theta - Z'\| - \|\Delta\| + \lambda \|\Delta\|^r \right] - \lambda \delta \\ &= \max_{\lambda \geq 0} \mathbb{E}_{\mathbb{P}'_n} [\min \{ \|\theta - Z'\|, \lambda \|\theta - Z'\|^r \}] - \lambda \delta \\ &= \max_{\lambda \geq 0} \frac{1}{n} \sum_{i=1}^n \min \{ \|\theta - z'_i\|, \lambda \|\theta - z'_i\|^r \} - \lambda \delta \\ &= \max \left( \frac{1}{n} \sum_{i=1}^{k(\theta)-1} \|\theta - z'_i\| + \frac{1}{n} \left( 1 - \frac{n\delta - \sum_{i=k(\theta)+1}^n \|\theta - z'_i\|^r}{\|\theta - z'_{k(\theta)}\|^r} \right) \|\theta - z'_{k(\theta)}\|, 0 \right) \end{aligned}$$

where the third equality follows from Lemma B.1 in Appendix B.1 and the fifth one is due to Lemma B.2 in Appendix B.1.  $\blacksquare$



Building upon the proof of Theorem 4.1, we can establish the following characterization of the rectified distribution. The concave cost function  $\|z - z'\|^r$  (with  $r \in (0, 1)$ ) plays a pivotal role in this context by endowing the perturbation with a distinctive long-haul structure. Intuitively, for each data point, we can only observe two possible scenarios: either the perturbation is zero, indicating no movement or the data point is adjusted to eliminate the loss. In this process, the rectified data points are automatically identified as outliers and subsequently rectified.

**Proposition 4.2** (Characterization of Rectified Distribution). Assuming the same conditions as stated in Theorem 4.1, we can conclude that the optimal distribution  $\mathbb{Q}^*$

$$\mathbb{Q}^*(dz) = \frac{1}{n} \sum_{i=1}^{k(\theta)-1} \delta_{z'_i}(dz) + \frac{\eta}{n} \delta_{z'_{k(\theta)}} + \frac{n - k(\theta) + 1 - \eta}{n} \delta_\theta(dz)$$

where  $\eta = 1 - \frac{n\delta - \sum_{i=k(\theta)+1}^n \|\theta - z'_i\|^r}{\|\theta - z'_{k(\theta)}\|^r}$ . □

**Remark 4.2.** The existence of optimal solutions can then be directly applied from (Yue et al., 2022, Theorem 2). □

## 4.2 Least Absolute Deviation (LAD) Regression and More General Forms

Following the same technique, we can also derive the least absolute deviation case.

**Theorem 4.2** (LAD Regression). Suppose that  $\mathcal{Z} := \mathcal{X} \times \mathcal{Y} = \mathbb{R}^{d+1}$ ,  $\ell(\theta, z) = \|y - \theta^T x\|$  and the cost function is defined as  $c(z, z') = \|z - z'\|^r$  where  $r \in (0, 1)$  and  $\|\cdot\|$  is the  $\ell_2$  norm. Without loss of generality, suppose that  $\|y'_1 - \theta^T x'_1\| \leq \|y'_2 - \theta^T x'_2\| \leq \dots \leq \|y'_n - \theta^T x'_n\|$ , we have

$$\begin{aligned} & \min_{\mathbb{Q} \in \mathcal{R}(\mathbb{P}'_n)} \mathbb{E}_{\mathbb{Q}}[\|Y - \theta^T X\|] \\ &= \max \left( \frac{1}{n} \sum_{i=1}^{k(\theta)-1} \|y'_i - \theta^T x'_i\|^r + \frac{1}{n} \left( 1 - \frac{n\delta' - \sum_{i=k(\theta)+1}^n \|y'_i - \theta^T x'_i\|^r}{\|y'_{k(\theta)} - \theta^T x'_{k(\theta)}\|^r} \right) \|y'_{k(\theta)} - \theta^T x'_{k(\theta)}\|, 0 \right), \end{aligned}$$

where  $k(\theta) := \max_{k \in [n]} \{k : \frac{1}{n} \sum_{i=k}^n \|y'_i - \theta^T x'_i\|^r \geq \delta'\}$  and  $\delta' = \delta \|(\theta, -1)\|^r$ . □

*Proof.* The proof follows a similar idea to that of Theorem 4.1. For any fixed  $\theta$ , we can always sort  $\{z'_i\}_{i=1}^n$  based on the error  $\|y'_i - \theta^T x'_i\|$  to satisfy the condition. For simplicity, we denote  $\tilde{\theta} = (\theta, -1)$  and  $z = (x, y)$ . By the strong duality result in Proposition 4.1, we have

$$\begin{aligned} \min_{\mathbb{Q} \in \mathcal{R}(\mathbb{P}'_n)} \mathbb{E}_{\mathbb{Q}}[\|Y - \theta^T X\|] &= \max_{\lambda \geq 0} \mathbb{E}_{\mathbb{P}'_n} \left[ \min_{\Delta \in \mathbb{R}^{d+1}} \|\tilde{\theta}^T Z\| + \lambda \|\Delta\|^r \right] - \lambda \delta \\ &= \max_{\lambda \geq 0} \mathbb{E}_{\mathbb{P}'_n} \left[ \min_{\Delta \in \mathbb{R}^{d+1}} \|\tilde{\theta}^T Z' + \tilde{\theta}^T \Delta\| + \lambda \|\Delta\|^r \right] - \lambda \delta \\ &\stackrel{(a)}{=} \max_{\lambda \geq 0} \mathbb{E}_{\mathbb{P}'_n} \left[ \min_{\substack{\|\Delta\| \leq \frac{\|\tilde{\theta}^T Z'\|}{\|\tilde{\theta}\|_*}}} \|\tilde{\theta}^T Z'\| - \|\tilde{\theta}\|_* \|\Delta\| + \lambda \|\Delta\|^r \right] - \lambda \delta \\ &\stackrel{(b)}{=} \max_{\lambda \geq 0} \mathbb{E}_{\mathbb{P}'_n} \left[ \min \left\{ \|\tilde{\theta}^T Z'\|, \frac{\lambda \|\tilde{\theta}^T Z'\|^r}{\|\tilde{\theta}\|_*^r} \right\} \right] - \lambda \delta \end{aligned}$$

$$\begin{aligned}
&= \max_{\lambda \geq 0} \frac{1}{n} \sum_{i=1}^n \min \left\{ \|\tilde{\theta}^T z'_i\|, \frac{\lambda \|\tilde{\theta}^T z'_i\|^r}{\|\tilde{\theta}\|_*^r} \right\} - \lambda \delta \\
&\stackrel{(c)}{=} \max \left( \frac{1}{n} \sum_{i=1}^{k(\theta)-1} \|\tilde{\theta}^T z'_i\| + \frac{1}{n} \left( 1 - \frac{n\delta^r - \sum_{i=k(\theta)+1}^n \|\tilde{\theta}^T z'_i\|^r}{\|\tilde{\theta}^T z'_{k(\theta)}\|^r} \right) \|\tilde{\theta}^T z'_{k(\theta)}\|, 0 \right),
\end{aligned}$$

where the third equality follows from the Holder inequality and  $\|\cdot\|_*$  is the dual norm of  $\|\cdot\|$ ; the fourth one follows from Lemma B.1 and the sixth one is due to Lemma B.2.

This completes our proof. ■

The structure of the optimal rectified distribution also resembles Proposition 4.2. The rectified data points are shifted towards the hyperplane  $y = \theta^T x$  that best fits the clean data points.

**Extension to more general cases.** The proposed rectification set has the potential for broader applicability across various applications and problem domains. This versatility makes the rectification set a valuable tool for addressing and improving solutions in diverse problem settings in the future.

(i) **(Concave cost function)** From Proposition 4.1, the optimal rectification admits  $z_{\text{best}} \in \arg \min_{z \in \mathcal{Z}} \ell(\theta, z') + \lambda c(z, z')$ . Suppose we select a concave cost function  $c$  that grows strictly slower than the loss function  $\ell$ . In this scenario, when the budget is small, the rectified data point  $z_{\text{best}}$  consistently exhibits the long-haul structure, ensuring automatic outlier identification properties. This implies that the rectification process effectively identifies outliers, as the influence of the cost function dominates over the loss function for small budgets. To further illustrate the concept, we can consider a linear regression problem with the squared loss function  $\ell(\theta, z) = (y - \theta^T x)^2$  or a nonlinear loss using the  $r$ -th norm as the cost function. We refer the readers to Appendix B.2.

(ii) **(Other distribution metric/discrepancy)** Based on the two examples discussed earlier, we can infer that the optimal transport distance-based rectification set is particularly suitable for regression or problems with continuous response variables. This is because the budget  $\delta$  is used to compensate for the loss caused by identified outliers. However, in classification tasks, where the loss function may be less sensitive, the effectiveness of the optimal transport distance-based approach may be limited. To address this limitation and complement the rectification set for classification tasks, an alternative approach is to use  $\phi$ -divergences. This approach has already been proposed in a study by (Chen & Royset, 2022) for handling outliers in image classification tasks. The  $\phi$ -divergence-based rectification set operates by adjusting the weight assigned to outliers, effectively minimizing their impact on the overall data set. By reducing the weight placed on the detected outliers, the rectification set aims to remove their influence from the data set. This selective adjustment allows for the identification and removal of outliers, leading to a more refined and reliable data set.

### 4.3 Computational Procedure

Solving the optimization problems in the prior sections can be complicated, as in general, the minimization of a class of convex functions often leads to non-convex problems.

This issue becomes even more critical when dealing with our estimation problem, as these problems lack of weak convexity and is even not subdifferential regular, see (Clarke, 1990, Definition 2.3.4). Consequently, certain calculus rules, like the summation and chain rules, as referenced in (Rockafellar & Wets, 2009, Theorem 10.31). Consequently, computing a first-order oracle (specifically, a subgradient under any subdifferential

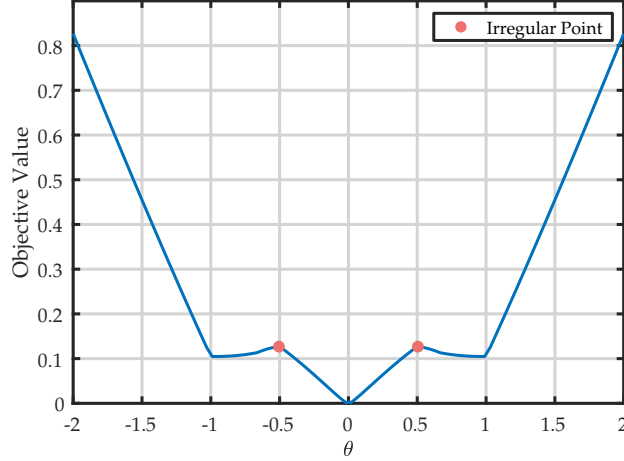


Figure 3: Irregular objective function.

concept, e.g., Fréchet, Limiting and Clarke subdifferentials ) with respect to  $\theta$  can prove to be challenging and practically intractable.

To concretely illustrate this challenge, we note that, intuitively, the graph of a subdifferentially regular function cannot exhibit "downward-facing cusps" (Li et al., 2020; Davis et al., 2020). Here, we give an example of when the objective function (4.2) is not regular, which may occur in general.

**Example 4.1** (Irregular Case (Three Point Masses)). Let  $\mathbb{P}'_n = \frac{1}{3}\delta_{-1} + \frac{1}{3}\delta_0 + \frac{1}{3}\delta_1$  and  $\delta = 0.7$ . Based on the reformulation result given in Theorem 4.1, we can plot the curve of the loss function from our proposed estimator, see Figure 3.  $\square$

From Figure 3, it is evident that there are at least two regions with "downward-facing cusps" (marked as irregularities in the figures), which could potentially pose computational challenges. Similar challenges arise in the training of deep neural networks due to the ReLU activation function. However, the pseudo-subgradient (the subgradient we compute when assuming the chain rule holds or the back-propagation methods) remains effective for training the deep neural network empirically. In our empirical investigation, we have observed a similar phenomenon for our estimator.

Our procedure is following the calculus rule. In each iteration, given the current estimate  $\theta$ , we compute the optimal rectified distribution. For simple applications such as mean estimation and least absolute deviation regression, we can solve this optimization problem efficiently using the quick-select algorithm or by utilizing an existing solver for linear programs to obtain the optimal solution for the dual variable  $\lambda$ , which we denote  $\lambda^*$ . Then, we employ the pseudo-subgradient method on the rectified data, iterating until convergence. This optimization process automatically rectifies outliers using a fixed budget  $\delta$  across all iterations. As the value of  $\theta$  changes, the same budget  $\delta$  for all iterations results in varying the quantile used for selecting outliers. Thus, our estimator can be regarded as an iteratively adaptive quantile estimation approach.

#### 4.3.1 Mean estimation and LAD regression procedure

We now concretely detail the procedure for LAD regression. The procedure for mean estimation is analogous and results from a simple change in the loss function. We must start by initially addressing the computation of the optimal dual variable  $\lambda^*$  for the inner minimization over the probability space. Without loss of generality, we recall that this problem is

$$\max_{\lambda \geq 0} \frac{1}{n} \sum_{i=1}^n \min \left\{ \|\tilde{\theta}^T z'_i\|, \frac{\lambda \|\tilde{\theta}^T z'_i\|^r}{\|\tilde{\theta}\|_*^r} \right\} - \lambda \delta. \quad (4.3)$$

We show in the Appendix in Section B.1 by Lemma B.2 that this problem can be solved by applying the quick-select algorithm to find the optimal  $\lambda^*$ . Applying this lemma yields our estimation approach, which is described in Algorithm 1.

---

**Algorithm 1:** Statistically Robust Estimator

---

**Data:** Observed data  $\{z'_i\}_{i=1}^n$ , initial point  $\theta_0$ , stepsizes  $\alpha_t > 0$ ;  
**1 for**  $t = 0, \dots, T$  **do**  
**2**     1. **Sort** the observed data  $\{z'_i\}_{i=1}^n$  via the value  $\|y'_i - \theta_t^T x'_i\|$ .  
**3**     2. **Quick-Select** algorithm to get the knot point  $k(\theta_t)$  and the optimal  $\lambda^*$ ;  
**4**     3. **Subgradient step** on the detected clean data:  

$$\theta_{t+1} = \theta_t - \frac{\alpha_t}{n} \sum_{i=1}^{k(\theta_t)} \text{sgn}(\theta_t^T x'_i - y'_i) \cdot x'_i$$
  
**5 end**

---

**Remark 4.3** (Alternative procedure for  $k(\theta_t)$  and  $\lambda^*$ ). It is illuminating to note that steps 1 and 2 in Algorithm 1 can be alternatively replaced with steps that solve a specific linear program for the knot point  $k(\theta_t)$  and optimal  $\lambda^*$ . Instead of applying the sorting and quick-select algorithm implied by Lemma B.2, we can instead reformulate Equation (4.3) as a linear programming problem, i.e.,

$$\begin{aligned} \max_{\lambda \geq 0, t \in \mathbb{R}^n} \quad & \frac{1}{n} \sum_{i=1}^n t_i - \lambda \delta \\ \text{s. t.} \quad & t_i \leq \|\tilde{\theta}^T z'_i\|, \forall i \in [n] \\ & \|\tilde{\theta}\|_*^r t_i \leq \lambda \|\tilde{\theta}^T z'_i\|^r, \forall i \in [n]. \end{aligned} \quad (4.4)$$

The problem in (4.4) can then be solved instead of carrying out steps 1 and 2 of Algorithm 1 to find the knot point  $k(\theta_t)$  and the optimal  $\lambda^*$ .  $\square$

### 4.3.2 General computational procedure

We also propose a procedure for fitting more general regression models with our statistically robust estimator which is based on the approach for LAD regression above.

Although the procedure can be applied to any model which can be estimated via subgradient methods, we focus on deep learning models. We start by considering a neural network  $f_\theta$  parameterized by weights  $\theta$ , and a loss function  $\ell(\theta, z) = \ell(y, f_\theta(x))$ , where  $\ell$  is a gradient Lipschitz function with a constant  $L$ . By Proposition 4.1, we would like to solve the inner problem

$$\max_{\lambda \geq 0} \mathbb{E}_{\mathbb{P}'_n} \left[ \min_{z \in \mathcal{Z}} \ell(\theta; Z') + \lambda c(z, Z') \right] - \lambda \delta. \quad (4.5)$$

Although we do not prove a reformulation result for this problem, we solve the problem empirically by employing a computational procedure which is analogous to that of LAD regression. The procedure is

heuristic and does not enjoy the same guarantees as Algorithm 1 does for LAD regression, but in experiments (see Section 6.2), we find that the performance is similarly robust to outliers and significantly outperforms benchmark models trained under empirical risk minimization. Our computational procedure follows in Algorithm 2.

---

**Algorithm 2:** Statistically Robust Optimization Procedure

---

**Data:** Observed data  $\{z'_i\}_{i=1}^n$ , initial point  $\theta^{(0)}$ , stepsizes  $\alpha^{(t)} > 0$ , sampling distribution  $\mathbb{P}'_n$ ; batch size  $m \leq n$ .

1 **for**  $t = 0, \dots, T$  **do**

2     1. **Sample**  $m$  points  $\{z'_i\}_{i=1}^m \sim \mathbb{P}'_n$ .

3     2. **Sort** the observed data  $\{z'_i\}_{i=1}^m$  via the value  $\ell(\theta^{(t)}, z'_i)$ .

4     3. **Quick-Select** algorithm to get the knot point  $k(\theta^{(t)})$  and the optimal  $\lambda^*$ .

5     4. **Subgradient step** on the detected clean data:

$$\theta^{(t+1)} = \theta^{(t)} - \alpha^{(t)} \sum_{i=1}^{k(\theta^{(t)})} v^*(\theta^{(t)}, z'_i)$$

      where  $v^*(\theta^{(t)}, z'_i) \in \partial_{\theta} \ell(\theta^{(t)}, z'_i)$ .

6 **end**

---

Algorithm 2 is similar to Algorithm 1, but has two principal differences: (1) instead of optimizing over the entire data set, we optimize over mini-batches of size  $m \leq n$  which are drawn from a data set of size  $n$  via a sampling distribution  $\mathbb{P}'_n$ ; and (2) instead of taking the pseudo-subgradient with respect to  $\theta$  for the LAD regression problem in calculating the direction of descent, we instead take a pseudo-subgradient with respect to  $\theta$  around each point  $z'_i$ , each of which is contained within the subdifferential  $\partial_{\theta} \ell(\theta^{(t)}, z'_i)$ . The pseudo-subgradient is in practice computed by the automatic differentiation capability of a software package such as Pytorch, Tensorflow, or JAX.

#### 4.3.3 Procedure for choosing $\delta$

The budget parameter  $\delta$  controls the quantile which identifies outliers in the algorithms above. However, these algorithms do not answer the question of how to select  $\delta$ . Although our simulations will show that our estimation is not especially sensitive to the choice of  $\delta$ , it is still useful to attempt to minimize the effect of the contamination in the observed distribution  $\mathbb{P}'$ . We now describe in broad terms cross-validation procedures for making this choice under specific cases in which additional data or preferences is available to be taken advantage of, and a general case which does not require these assumptions. The differentiation for specific cases is useful for improving performance in realistic situations when such additional resources are available, as they are in the next section.

**Procedure with small  $\epsilon$ .** When  $\epsilon$  is small, the probability of picking an outlier in a small sample from the contaminated distribution is small. The probability of drawing a sample of size  $m$  without an outlier is  $(1 - \epsilon)^m$ , and for small enough  $\epsilon$ , it is unlikely for the sample to contain an outlier. To ameliorate the effect of an unfortunate sample containing an outlier, several samples of size  $m$  can be made from the contaminated distribution and used for tuning  $\delta$ . The problem is easy and fast, as the length of the samples is very low. After computing the optimal  $\delta$  for each sample, a robust measure of location can be made (using

e.g. our estimator) to compute an estimate for the optimal  $\delta$ . Therefore, when  $\epsilon$  is small enough, the existing contaminated distribution can be sampled from to form a “pseudo-clean” validation set for tuning  $\delta$ .

**Procedure with time-varying  $\epsilon$ .** In this specialized procedure, we assume that each observation is observed as part of a discrete sequence with index  $t = 1, 2, \dots, n$ . In a small departure from our theoretical setup, we make an assumption that the observations up to  $n$  are not always drawn from a distribution with the same  $\epsilon$ . In short,  $\epsilon$  varies with time, taking on values of either 0 or  $\epsilon$  (i.e.  $\epsilon_t$  is a telegraph process). We assume that after time  $t = n$ ,  $\epsilon_t = 0$ . Thus our data-generating distribution contains some observations which are known to be free of corruption. These observations can then form a test set which is used to tune  $\delta$  in the typical manner via e.g.  $k$ -fold cross-validation.

**Procedure with a certificate function.** In this specialized procedure, we assume the availability of a “certificate function”. The certificate function is an algorithm which returns a boolean indicating whether or not the model performs adequately in cross-validation on the training data using an alternative measure of model fit which is informed by a domain expert. Standard cross-validation is used to tune  $\delta$  until the average of the certificate function over a data set is satisfied. An example of this approach could be utilized in the following experimental results in Section 6, in which we let the certificate function be the smoothness of an estimated surface which domain experts expect *a priori* to be smooth. An average smoothness which is lower than the average smoothness produced by a benchmark method (which is not resistant to corruption) would e.g. satisfy the certificate function.

**General procedure.** Although we expect most realistic applications of our approach to enjoy access to an estimate of  $\epsilon$ , a sequence of data which may sometimes be free of corruption, or a certificate function, certainly not all applications will fall into one of these cases. In these cases we find in experiments in Section 6.1 that typical cross-validation approaches can still be employed with reasonable effect for most  $\epsilon$ .

## 5 Experimental Results

In this section, we demonstrate the effectiveness of the proposed statistically robust estimator through various simulated tasks: mean estimation and LAD regression.

### 5.1 Mean Estimation

We generate the corrupted data by combining two Gaussian distributions:  $(1 - \text{corruption level}) \times \mathcal{N}(0, 2)$  and  $(\text{corruption level}) \times \mathcal{N}(25, 2)$ . All the results presented in Table 1 are the mean estimators and the confidence intervals (i.e. twice the standard deviation) are averaged over 100 random trials for different corruption levels. We compare our estimator with several widely used baseline methods. Interestingly, we observe that even when setting hyperparameters as constants across all corruption levels, our estimator consistently outperforms the others. Notably, the trimmed mean, which incorporates the ground truth corruption level, performs even worse than our estimator. Our estimator’s outperformance is notable, as in this table we report results specifically using  $\delta = 0.5$ , which is a non-optimal choice for  $\delta$ , as we will show in the sensitivity analysis below.

We visualize the corrupted distribution and its rectified distribution when the corruption level is 45% in Figure 4. In this case, 55% of the data is drawn from the true distribution  $\mathcal{N}(0, 2)$  and 45% is drawn from  $\mathcal{N}(25, 2)$ . Figure 4(a) displays the original sample of data from the contaminated distribution. The



Corruption Levels	20%	30%	40%	45%	49%
Mean	$5.009 \pm 0.056$	$7.509 \pm 0.080$	$10.007 \pm 0.098$	$11.248 \pm 0.098$	$12.257 \pm 0.114$
Median	$1.680 \pm 0.114$	$1.831 \pm 0.118$	$2.286 \pm 0.192$	$2.843 \pm 0.208$	$4.203 \pm 0.344$
Trimmed Mean	$1.739 \pm 0.108$	$1.947 \pm 0.104$	$2.456 \pm 0.212$	$3.047 \pm 0.174$	$4.399 \pm 0.360$
Ours	<b><math>1.620 \pm 0.106</math></b>	<b><math>1.700 \pm 0.106</math></b>	<b><math>1.957 \pm 0.160</math></b>	<b><math>2.251 \pm 0.150</math></b>	<b><math>2.899 \pm 0.240</math></b>
Ours, %Rectified	10.03%	10.12%	10.24%	10.35%	10.55%

Table 1: We compared our estimator with several standard mean estimation methods by evaluating the average loss on clean data points across various corruption levels. In our evaluation, we set the percent level of trimmed mean equal to the unknown ground truth corruption level. The hyperparameters for our estimator, namely  $\delta = 0.5$  and  $r = 0.5$ , remained constant across all corrupted levels. The last row in the comparison table represents the percentage of all points rectified by our method.

outlier points from the contaminating distribution are clearly visible in orange. Figure 4(b) shows the rectified distribution our estimator produces for  $\delta = 2.5$ , in which the outlier points have been moved from their original values to their rectified values, which is much closer to the true mean of the clean distribution. Our estimator thus successfully identifies the majority of outliers and relocates them towards the center (our mean estimator), providing further support for our theoretical findings in the previous section. The sensitivity analysis of mean estimation with respect to  $\delta$  is displayed in Figure 4(c). In this figure, the loss on the clean data is plotted for various values of  $\delta$ . We see that an approximate minimum occurs at  $\delta = 2$ , with good performance within the range  $\delta \in [0.5, 2.5]$ . This illustrates the relative insensitivity of our estimator to different values of  $\delta$  for a wide and reasonable range. This range can be easily reached by hyperparameter tuning via cross-validation, as the function describing the performance of our estimator is approximately quasiconvex. Moreover, when  $\delta = 0$  or when  $\delta$  is set so large that it can rectify all points, our estimator gracefully degrades to the loss of the median estimator, which is another favorable property. A further sensitivity analysis with respect to  $r$  is given in Section C.1 in the Appendix. In this sensitivity analysis we find a similarly wide region of good performance for  $r$  which improves significantly and almost uniformly on the more typical setting of  $r = 1$ .

The evolution of the rectified distribution for mean estimation under concave and convex cost functions as  $\delta$  increases is depicted in Appendices C.2 and C.3. These depictions show that our statistically robust estimator which applies the concave transport cost function acts in a stable and expected manner as  $\delta$  increases. In particular, this depiction shows that our estimator moves points in the order of their distance from the estimate of the mean; that is, the budget is “used” on the worst outliers first. This results in an orderly procedure of rectification which is stable and predictable across nearby values of  $\delta$ , which is a favorable property if  $\delta$  is being set sequentially or in cross-validation. In contrast, the estimator which applies the convex transport cost function moves all points of the clean and outlier distributions toward each other, which results in poor estimates of the true mean and an improper rectified distribution.

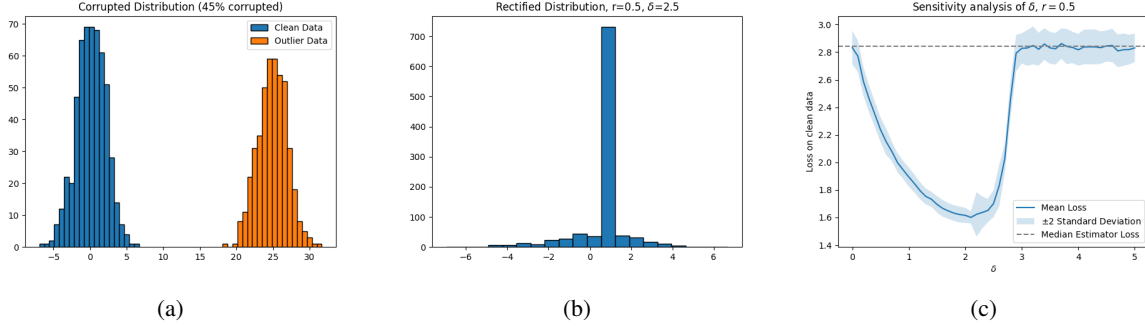


Figure 4: (a): Visualization of contamination model: a mixture of Gaussian  $0.55 \times \mathcal{N}(0, 2) + 0.45 \times \mathcal{N}(25, 2)$ ; (b): The rectified data generated by the proposed statistically robust estimator; (c) The sensitivity analysis of  $\delta$ . The visualization of (a) and (b) shows that the outlier points are rectified into the bulk of the clean distribution at  $\delta = 2.5$ . The sensitivity analysis of  $\delta$  shows that this rectification occurs for a wide range of  $\delta$  which leads to losses for mean estimation which are lower than that of the median estimator of location. As  $\delta \rightarrow 0$  and as  $\delta$  increases, the performance of our estimator gracefully degrades to that the median estimator.

## 5.2 LAD Regression

As we discussed in the previous result, the theoretical analysis for the LAD estimator resembles that of the mean estimation task. Empirically, we also observe similar performance for the LAD estimator and show that our estimator correctly rectifies most of outliers to the fitted hyperplane under a range of choices for  $\delta$ . In order to further support the effectiveness of our estimator, we provide additional visualizations: Figure 5 contains a visualization of the lines of best fit produced by various estimations to the LAD regression problem, and displays the effect of different choices of  $\delta$  on the line of best fit produced by our estimator. In Figure 5(a) our estimator with  $\delta = 1$  successfully produces a line of best fit which is closest to the uncontaminated distribution, while the other estimators (OLS, LAD, and Huber regressors) produce lines which are heavily affected by the contaminating distribution, showcasing the robustness of our estimator. Figure 5(b) and 5(c) show the rectified distribution produced by our estimator under  $\delta = 1$  (b) and  $\delta = 1.5$  (c). The suboptimal value of  $\delta = 1$  still rectifies many points from the contaminated distribution and produces a good line of best fit. Setting  $\delta = 1.5$  rectifies all of the points from the contaminated distribution and essentially recovers the true line of best fit. Importantly, this simulation shows that even improperly setting  $\delta$  to the suboptimal value of  $\delta = 1$  produces a much better line than any of the other estimators in Figure 5(a). Appendix C.4 contains comparisons over different random trials and a sensitivity analysis with respect to  $\delta$  and  $r$ , along with experimental results from our cross-validation approach.

## 6 Empirical Studies

In this section, we conduct empirical studies on real-world applications in fitting and predicting option implied volatility surfaces.

Options are financial instruments that grant the buyer the choice to buy or sell an asset at a predetermined price in the future. Those which grant buying privileges are referred to as call options, and those which grant sale privileges are referred to as put options. The predetermined price at which the underlying asset may be purchased or sold is known as the strike price. The option has an expiration date and time at which it expires.

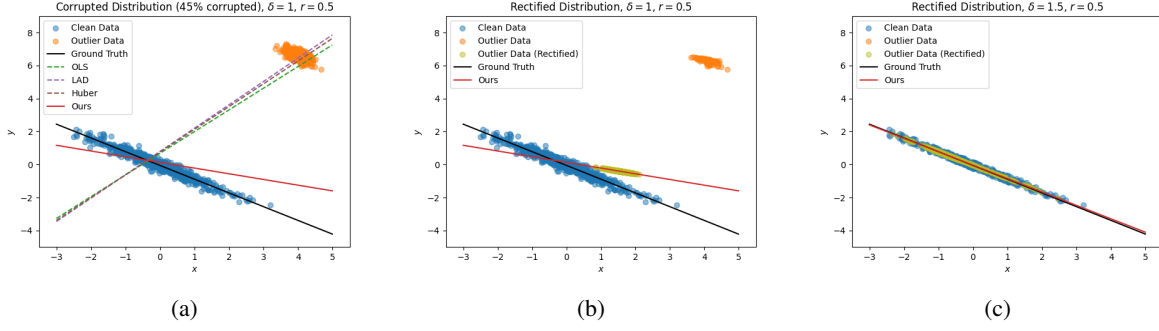


Figure 5: (a): Visualization of contamination model: 55% are drawn with  $x \sim \mathcal{N}(0, 2)$  and  $y = 0.1 - 0.8x + 0.2w$ . 45% are drawn with  $x \sim \mathcal{N}(4, 2)$  and  $y = 10.1 - 0.8x + 0.2w$ . In each case  $w \sim \mathcal{N}(0, 1)$ . Fitted models for different baselines are: OLS (ordinary least square), LAD (least absolute deviation regression), Huber (Huber regression with threshold parameter 1.5); (b): The rectified data generated by the proposed statistically robust estimator with a small budget  $\delta = 1$ ; (c): The rectified data with a larger  $\delta = 1.5$  is able to rectify all outliers.

The remaining time until this point is referred to as the time to maturity. Options markets recognize various styles of exercising the right to buy or sell. In this empirical study, we only work with European-style options, in which exercise is only allowed at the expiration time. European options are broadly traded and analyzed in financial markets and are one of the most popular styles of options traded globally.

Option prices are generally impacted by the volatility of the underlying asset’s price process. The implied volatility (IV) is a measure derived from an option’s market price, reflecting the volatility expectation of the underlying asset’s price. The implied volatility surface (IVS) is the variation of implied volatility across options with different strike prices and times to maturity. The IVS is important in quantitative finance for risk assessment, hedging, pricing, and trading decisions (Cont & Da Fonseca, 2002; Daglish et al., 2007; Kamal & Gatheral, 2010; Gatheral, 2011). However, outliers in implied volatilities can distort the IVS and lead to inaccurate estimation. Consequently, there is a need for robust option implied volatility surface methods. Our approach handles this issue by estimating the surface in the presence of outliers. In this section, we perform two experiments which illustrate the efficacy of our statistically robust estimator for (a) estimating the IVS given options chains using a kernelized IVS estimator, and (b) estimating the IVS given options chains using a state-of-the-art deep learning IVS estimator.

## 6.1 Kernelized Volatility Surface Estimation

**Data.** Our data set consists of nearly 2,000 option chains containing end-of-day option prices from the US stock market, spanning the years 2019–2021. The options data comes from OptionMetrics via WRDS, a financial research data service available to major research universities. The chains chosen were identified as containing significant outliers by our industry partner, firm providing global financial data and analysis. We randomly divide each option chain into an 80% train set and a 20% test set. Using the train set, we estimate surfaces and evaluate their out-of-sample performance using mean absolute percentage error (MAPE) and the discretized surface gradient (defined as  $\nabla \hat{S}$ ), a measure of surface smoothness. The MAPE evaluates the error of the options price surface when compared against the observed option implied volatilities.  $\nabla \hat{S}$  evaluates the smoothness of the estimated surface. Further details of the data set can be found in Appendix C.8.

**Losses.** These losses are chosen for their importance in finance and option trading and valuation. MAPE is a preferable error metric for volatility surfaces, as option chains contain options with implied volatilities which can differ in orders of magnitude, and MAPE weighs equally the contribution to error of options with such volatilities. The discretized surface gradient  $\nabla \hat{S}$  measures surface smoothness of the estimated volatility surface by computing a discrete gradient across a grid of points in the (time to expiration, strike price) plane. Smooth surfaces are important for several reasons: (1) smoother surfaces allow more stable interpolation or extrapolation of implied volatility for options with market prices which are not directly observable; (2) smoother surfaces produce smaller adjustments for option hedging positions constructed from measures of the IVS, which ultimately lowers hedging transaction costs; (3) smoother surfaces are less likely to have internal arbitrages between options, which are implied by sharp discontinuities in the IVS, putting the surface more in line with established asset pricing theory; and (4) smoother surfaces produce more stable estimates of financial institutions’ derivative exposures, which are required to be consistent for financial regulatory and reporting requirements. These measures are standard in options IVS estimation, and further details on their definition can be found in Appendix C.8.

**Benchmarks.** We compare the kernelized statistically robust estimator developed in Theorem 4.2 to two benchmarks. The first is kernel smoothing (denoted “KS”), a well-established method for estimating the IVS (Aït-Sahalia & Lo, 1998). In kernel smoothing, each point on the IVS is constructed by a weighted local average of implied volatilities across nearby expiration dates, strike prices, and call/put type. The weights are given by a kernel matrix which depends on these three features of an option. The second benchmark is a two-step kernel smoothing method (denoted “2SKS”) which attempts to specially treat outlier points before estimating with the KS method. In this two-step method, options in an options chain are removed if their implied volatilities fall outside of the region  $[q_{0.25} - 1.5 \cdot IQR, q_{0.75} + 1.5 \cdot IQR]$ , where  $q_{0.25}$  is the 25% quantile of the implied volatilities in the options chain,  $q_{0.75}$  is defined similarly, and IQR is the interquartile range of the implied volatilities in the options chain. The surface is then estimated upon the remaining options via the KS method. This two-step “remove and fit” method is a well-known method for fitting models under outliers; the outlier identification procedure is commonly known as Tukey Fences (Hoaglin et al., 1986).

**Kernelized Regression Problem.** Following the convention in (Aït-Sahalia & Lo, 1998), the  $i$ th option in a chain is featurized as the vector  $\mathbb{R}^3 \ni x'_i = (\log \tau_i, u(\Delta_i), \mathbb{1}_{\text{call}(i)})$ , where  $\tau_i$  is the number of days to the option’s expiration date,  $\Delta_i \in [-1, 1]$  is a relative measure of price termed the Black-Scholes delta,  $u(x) = x\mathbb{1}_{x \geq 0} + (1 + x)\mathbb{1}_{x < 0}$ , and  $\mathbb{1}_{\text{call}(i)}$  is 1 if the option is a call option and 0 if the option is a put option. The goal is to fit the pair  $(y'_i: \text{the implied volatility of option } i, x'_i: \text{the features})$  via a kernelized regression model. We choose a Gaussian-like kernel  $K_h(x, x')$  to measure the distance between options  $x$  and  $x'$  as  $K_h(x, x') = \exp(-\|(x - x')/2h\|^2)$  where division of  $x - x'$  by  $h$  is element-wise for a vector of bandwidths  $h \in \mathbb{R}_+^3$ . When the budget  $\delta = 0$ , we want to solve  $\min_{\theta \in \mathbb{R}^n} \sum_{i=1}^n v_i |y'_i - \theta^T K_h^i|$ , where  $v_i$  is the  $i$ -th entry of a vector of vegas for  $\{x'_i\}_{i=1}^n$  and  $K_h^i$  is the  $i$ -th row of the kernel matrix. The implied volatilities are weighted by vega  $v_i$  to improve surface stability as in (Mayhew, 1995). We conducted a comparison between our estimator and the benchmarks. We note that the KS method can be regarded as a standard kernelized least square approach (Hansen, 2022).

**Results.** Our approach improves upon the benchmark approach in both MAPE and  $\nabla \hat{S}$  on the out-of-sample test sets, showcasing the importance of jointly estimating the rectified distribution and model parameters with our estimator. The results of our experiment are displayed in Table 2. We compare the KS and 2SKS benchmarks against our estimator with a fixed  $\delta = 0.01$  (chosen to correspond to a 1% change in volatility)

and  $\delta$  chosen by cross-validation, which is used to tune  $\delta$  for each option chain. Details of the cross-validation procedure can be found in Appendix C.8.

Our estimator attains a mean MAPE of 0.225 across all chains, while the KS estimator and 2SKS estimator attain mean MAPEs of 0.294 and 0.236, respectively. The quantiles and mean of each estimator is reported in the upper section of Table 2 below. Our estimator thus improves upon the existing MAPE by 23% for the non-robust benchmark and 5% for the robust benchmark, illustrating the efficacy of our novel statistically robust estimator. The lower section of Table 2 reports the smoothness results of the estimated surfaces. Our estimator attains a mean  $\nabla \hat{S}$  of 6.5 versus a mean of 20.2 for the KS estimator and 7.5 for the 2SKS estimator. This corresponds to improvements of 67% and 13%, respectively, demonstrating that outlier rectification is important for producing smooth surfaces which can be used in financial applications.<sup>1</sup>

Model MAPE	0.5% Quantile	5% Quantile	Median	Mean	95% Quantile	99.5% Quantile
KS	0.026	0.068	0.232	0.294	0.677	1.438
2SKS	0.026	0.056	0.172	0.236	0.602	1.389
Ours ( $\delta = 10^{-2}$ )	0.028	0.057	0.170	0.225	0.535	1.207
Ours (CV)	0.028	0.057	0.169	0.224	0.534	1.240

Model $\nabla \hat{S}$	0.5% Quantile	5% Quantile	Median	Mean	95% Quantile	99.5% Quantile
KS	0.313	1.606	14.434	20.188	57.797	108.901
2SKS	0.050	0.124	2.229	7.491	33.276	78.144
Ours ( $\delta = 10^{-2}$ )	0.048	0.121	1.898	6.502	28.064	66.410
Ours (CV)	0.043	0.109	1.513	5.079	21.096	55.005

Table 2: This table reports the mean and quantiles of the distribution of MAPE and  $\nabla \hat{S}$  across all option chains for the benchmark KS and 2SKS methods, and our estimator under  $\delta = 0.01$  and  $\delta$  set via cross-validation. Our estimator achieves lower MAPE in many cases than the two benchmark approaches, and achieves much lower  $\nabla \hat{S}$  than the benchmark estimators. Applying cross-validation generally improves smoothness, while maintaining similar MAPE. The improvement of our estimator over the benchmarks illustrates the importance of rectifying outliers for IVS estimation.

To contextualize these results, we note that the difference in MAPE of a surface and an option chain containing outliers and the MAPE of a surface and an option chain containing no outliers will not be large if the set of outliers is small. Consider the MAPE of the same surface for two different option chains of size  $n$ ,  $O_1$  and  $O_2$ , where a small fraction  $k/n$  of the options of  $O_2$  are outliers. Supposing the modal APE is 0.3 and the outlier APE is a considerable 1.0, for an options chain with  $n = 50$  and just  $k = 5$ , the MAPE difference will be only  $\frac{k+0.3(n-k)}{n} - 0.3 = 0.07$ .

We perform an additional experiment with the same dataset in Appendix C.7 which demonstrates the

<sup>1</sup>It is notable to report that applying our estimator to an additional, completely out-of-sample test set collected after this paper was written allowed our industry partner to estimate and release to production 25% more surfaces than they had before when using their existing proprietary method.

usefulness of our method for estimating an IVS for use on the trading day after the initial contaminated surface is observed. We find similar outperformance of our method versus the benchmark methods, with improvements in MAPE and  $\nabla \hat{S}$ . This experiment shows that our method is successful in interpolating as well as predicting the IVS in the presence of outliers.

## 6.2 Deep Learning Volatility Surface Estimation

In this section, we apply our statistically robust estimator to state-of-the-art deep learning prediction approaches for volatility modeling developed in [Chataigner et al. \(2020\)](#). We show that our estimator improves upon the performance of state of the art methods when faced with data containing outliers.

**Background.** IVS estimation provides an approximate surface fit for the volatilities implied by option market prices. However, market participants often require surfaces which fit as closely as possible to the market-implied volatilities.<sup>2</sup> One of the most popular methods used in mathematical finance to estimate surfaces obeying such a constraint under a reasonable stochastic process model for the evolution of asset prices is the *local volatility* or *implied volatility function* model introduced by [Rubinstein \(1994\)](#), [Dupire et al. \(1994\)](#), and [Emanuel Derman & Zou \(1996\)](#). The local volatility model assumptions imply that a function  $\sigma(K, T)$  exists which gives an analytic expression for the volatility  $\sigma$  at a given option strike price  $K$  and option time to expiration  $T$ . This function is known as Dupire’s formula after its originator. Enforcing Dupire’s formula in the estimation of a surface results in a local volatility surface, which is of great use to financial market participants. However, estimating such a surface becomes significantly complicated if market data contains corruptions or unrealistic outliers which are unlikely to occur in the future.<sup>3</sup> As human intervention for outlier rectification in a large number of IVS fitting tasks is unrealistic, an automatic method for rectifying outliers in models fitting local volatility surfaces is required.

**Data.** We utilize the data set of [Chataigner et al. \(2020\)](#), which contains 17 (options chain, IVS) pairs taken from the German DAX index in August 2001. Options chains are captured from daily options market data, and IVSes are estimated for a grid of strikes and maturities via a trinomial tree calibrated by the method of [Crépey \(2002\)](#). In addition to [Chataigner et al. \(2020\)](#), this data set is also used in [Crépey \(2002\)](#) and [Crépey \(2004\)](#). In this data set’s usage in the literature, the authors train and test using the price surface, which is given by a nonlinear transformation of the IVS. Consequently, we also use the price surface for fitting; however, we report results after transforming back to the IVS. To corrupt the data set, a percentage of the options in each options chain are selected. We refer to this percentage, the corruption level, as  $\epsilon$ . The prices of these options  $x$  are then corrupted by replacing them with the values  $10x$ .

**Benchmark Method.** As a benchmark, we apply the state-of-the-art deep learning approach from [Chataigner et al. \(2020\)](#), the Dupire neural network. In this approach, a neural network estimates the price surface under the local volatility model assumptions encoded in Dupire’s formula, and additional no-arbitrage constraints which are useful for empirical applications. These conditions are enforced using different approaches: hard, split, and soft constraints. Hard constraints enforce the conditions by separating the network into subnetworks which have separate input layers for the variables involved in each of the conditions; conditions such as

<sup>2</sup>For example, banks pricing some kinds of exotic options require such surfaces to avoid arbitrage opportunities in surfaces that their internal trading teams may exploit, as outlined in [Hull & Basu \(2022\)](#). Participants pricing options may moreover simply prefer to accept the assumption that the market prices are usually correct, and thus prefer closely fitting surfaces.

<sup>3</sup>This may occur due to low liquidity, which allows market manipulation or adversarial trading to produce unrealistic prices.



convexity and non-negativity are then enforced by projection steps during optimization and the proper choice of activation functions. Hard constraints thus learn a function which explicitly satisfies the conditions. Soft constraints enforce these conditions instead by penalizing violations of them at each of the training points observed from the market. Hybrid constraints split the network into subnetworks which have separate input layers for each of the constrained variables as in hard constraints, and utilize soft constraints for enforcing the Dupire and no-arbitrage conditions. The function learned only approximately satisfies the conditions in theory, but in practice the approximation is very good (see [Chataigner et al. \(2020\)](#) for details). Because these approaches estimate the price surface, we also estimate the price surface in this application; however, the local volatility surface is easily recovered from the price surface by a nonlinear transformation.

**Robust Neural Network Estimation Problem.** To estimate price and volatility surfaces under the induced corruption, we estimated the benchmark approach using our statistically robust estimator. For each options chain, we tune  $\delta$  using the cross-validation procedure outlined in the general procedure of Section 4.3.3 in the following way: for each day, we sample 80% of the training set without replacement as a cross-validation (CV) training set, and use the remaining 20% of the training set as a CV validation set. We then train our robust neural network estimator on the CV training set with  $\delta \in \{10^{-3}, 10^{-2}, \dots, 10^3\}$ . For each  $\delta$ , we then compute the MAPE on the CV validation set. We then select the  $\delta$  with the lowest MAPE on CV validation set, and we use this  $\delta$  to train our estimator on the entire training set. This produces our final estimated model.

**Results.** To maintain comparability with the benchmark, we test and report the same metrics reported by [Chataigner et al. \(2020\)](#), namely, the RMSE and MAPE for the surface estimation. The metrics for each day and model are repeated for three trials with different random weight initialization seeds. The results are displayed in Table 3 below. The first panel displays the RMSE and MAPE for each model using the different constraint techniques, averaged across all trials and corruption levels. The second panel displays the RMSE and MAPE for each corruption level averaged across all models. Our approach outperforms the baseline approach across all averages, and does so more clearly as the corruption level increases, despite the strong regularizing effect of the no-arbitrage constraints and enforcement of Dupire’s formula. Our improvement is present across all models, and is especially impactful for the most accurate model utilizing soft arbitrage constraints. For this model, the out-of-sample test error in terms of RMSE and MAPE are reduced by 33% and 34%, respectively. This experiment displays the efficacy of our estimator in a state-of-the-art deep learning model for option price surface modeling.

## 7 Conclusion

In conclusion, we propose an automatic outlier rectification mechanism that integrates outlier correction and estimation within a unified optimization framework. Our novel approach leverages the optimal transport distance with a concave cost function to construct a rectification set within the realm of probability distributions. Within this set, we identify the optimal distribution for conducting the estimation task. Notably, the concave cost function’s ”long hauls” attribute facilitates moving only a fraction of the data to distant positions while preserving the remaining dataset, enabling efficient outlier correction during the optimization process. Through comprehensive simulation and empirical analyses involving mean estimation, least absolute regression, and fitting option implied volatility surfaces, we substantiate the effectiveness and superiority of our method over conventional approaches. This demonstrates the potential of our framework to significantly enhance outlier detection integrated within the estimation process across diverse analytical scenarios.

<b>Panel A: Results by Constraint Type</b>			
Model	Hard Constraints	Hybrid Constraints	Soft Constraints
Dupire NN RMSE	0.125	0.140	0.044
Our RMSE	0.110	0.131	0.029
Dupire NN MAPE	0.343	0.546	0.111
Our MAPE	0.310	0.508	0.074
<b>Panel B: Results by Corruption Level</b>			
Corruption Level	$\epsilon = 20\%$	$\epsilon = 30\%$	$\epsilon = 40\%$
Dupire NN RMSE	0.077	0.091	0.168
Our RMSE	0.075	0.084	0.141
Dupire NN MAPE	0.061	0.070	0.115
Our MAPE	0.060	0.066	0.097

Table 3: Mean RMSE and MAPE for implied volatility estimation across all samples for the benchmark deep learning approach and the deep learning approach estimated using our statistically robust estimator, split by constraint method (top Panel A) and corruption level (bottom Panel B). Our estimator achieves significantly lower RMSE and MAPE in estimating the implied volatility surface. Results for models are averaged across  $\epsilon \in \{0.2, 0.3, 0.4\}$ , and results for corruption levels are averaged across models using the hard, hybrid, and soft constraint methods.

## Acknowledgments

The material in this paper is based upon work supported by the Air Force Office of Scientific Research under award number FA9550-20-1-0397. Additional support is gratefully acknowledged from NSF 1915967, 2118199, 2229012, 2312204.

## References

- Yacine Aït-Sahalia and Andrew W Lo. Nonparametric estimation of state-price densities implicit in financial asset prices. *The Journal of Finance*, 53(2):499–547, 1998. 18
- Güzin Bayraksan and David K Love. Data-driven stochastic programming using phi-divergences. In *The operations research revolution*, pp. 1–19. INFORMS, 2015. 2
- Aharon Ben-Tal, Dick Den Hertog, Anja De Waegenaere, Bertrand Melenberg, and Gijb Rennen. Robust solutions of optimization problems affected by uncertain probabilities. *Management Science*, 59(2): 341–357, 2013. 2
- Jose Blanchet and Yang Kang. Distributionally robust groupwise regularization estimator. In *Asian Conference on Machine Learning*, pp. 97–112. PMLR, 2017. 2
- Jose Blanchet and Karthyek Murthy. Quantifying distributional model risk via optimal transport. *Mathematics of Operations Research*, 44(2):565–600, 2019. 7
- Jose Blanchet, Jiajin Li, Sirui Lin, and Xuhui Zhang. Distributionally robust optimization and robust statistics. *arXiv preprint arXiv:2401.14655*, 2024. 3
- George EP Box. Non-normality and tests on variances. *Biometrika*, 40(3/4):318–335, 1953. 2
- Marc Chataigner, Stéphane Crépey, and Matthew Dixon. Deep local volatility. *Risks*, 8(3):82, 2020. 20, 21
- Louis L Chen and Johannes O Royset. Rockafellian relaxation in optimization under uncertainty: Asymptotically exact formulations. *arXiv preprint arXiv:2204.04762*, 2022. 10
- Frank H Clarke. *Optimization and nonsmooth analysis*. SIAM, 1990. 10
- Rama Cont and José Da Fonseca. Dynamics of implied volatility surfaces. *Quantitative finance*, 2(1):45, 2002. 17
- Stéphane Crépey. Calibration of the local volatility in a trinomial tree using tikhonov regularization. *Inverse Problems*, 19(1):91, 2002. 20
- Stéphane Crépey. Delta-hedging vega risk? *Quantitative Finance*, 4(5):559–579, 2004. 20
- Toby Daglish, John Hull, and Wulin Suo. Volatility surfaces: theory, rules of thumb, and empirical evidence. *Quantitative Finance*, 7(5):507–524, 2007. 17
- Damek Davis, Dmitriy Drusvyatskiy, Sham Kakade, and Jason D Lee. Stochastic subgradient method converges on tame functions. *Foundations of computational mathematics*, 20(1):119–154, 2020. 11

- Erick Delage and Yinyu Ye. Distributionally robust optimization under moment uncertainty with application to data-driven problems. *Operations research*, 58(3):595–612, 2010. 2
- David L Donoho and Richard C Liu. The automatic robustness of minimum distance functionals. *The Annals of Statistics*, 16(2):552–586, 1988a. 2, 5
- David L Donoho and Richard C Liu. Pathologies of some minimum distance estimators. *The Annals of Statistics*, pp. 587–608, 1988b. 2
- Bruno Dupire et al. Pricing with a smile. *Risk*, 7(1):18–20, 1994. 20
- Iraj Kani Emanuel Derman and Joseph Z. Zou. The local volatility surface: Unlocking the information in index option prices. *Financial Analysts Journal*, 52(4):25–36, 1996. 20
- Rui Gao and Anton Kleywegt. Distributionally robust stochastic optimization with wasserstein distance. *Mathematics of Operations Research*, 2022. 2, 7
- Jim Gatheral. *The Volatility Surface: A Practitioner’s Guide*. John Wiley & Sons, 2011. 17
- Joseph Diez Gergonne. Dissertation sur la recherche du milieu le plus probable. *Etc. Annales math. pures appl*, 12(6):181–204, 1821. 1
- Frank R Hampel. *Contributions to the theory of robust estimation*. University of California, Berkeley, 1968. 2
- Frank R Hampel. A general qualitative definition of robustness. *The annals of mathematical statistics*, 42(6): 1887–1896, 1971. 2
- Bruce Hansen. *Econometrics*, chapter 19: Nonparametric Regression. Princeton University Press, 2022. 18
- Xuming He and Stephen Portnoy. Reweighted ls estimators converge at the same rate as the initial estimator. *The Annals of Statistics*, pp. 2161–2167, 1992. 2
- David C Hoaglin, Boris Iglewicz, and John W Tukey. Performance of some resistant rules for outlier labeling. *Journal of the American Statistical Association*, 81(396):991–999, 1986. 18
- Peter J Huber. Robust estimation of a location parameter. *Ann Math Stat*, 35:73–101, 1964. 2
- John Hull and Sankarshan Basu. 27.3: *The IVF Model*, pp. 659–660. Pearson, 11 edition, 2022. 20
- María Jaenada, Pedro Miranda, and Leandro Pardo. Robust test statistics based on restricted minimum rényi’s pseudodistance estimators. *Entropy*, 24(5):616, 2022. 2
- Nan Jiang and Weijun Xie. Distributionally favorable optimization: A framework for data-driven decision-making with endogenous outliers. *SIAM Journal on Optimization*, 34(1):419–458, 2024. 2, 5
- Michael Kamal and Jim Gatheral. Implied volatility surface. *Encyclopedia of quantitative finance*, 2010. 17
- Daniel Kuhn, Peyman Mohajerin Esfahani, Viet Anh Nguyen, and Soroosh Shafieezadeh-Abadeh. Wasserstein distributionally robust optimization: Theory and applications in machine learning. In *Operations research & management science in the age of analytics*, pp. 130–166. Informs, 2019. 2

- Jiajin Li, Anthony Man-Cho So, and Wing-Kin Ma. Understanding notions of stationarity in nonsmooth optimization: A guided tour of various constructions of subdifferential for nonsmooth functions. *IEEE Signal Processing Magazine*, 37(5):18–31, 2020. 11
- Jiajin Li, Sirui Lin, Jose Blanchet, and Viet Anh Nguyen. Tikhonov regularization is optimal transport robust under martingale constraints. In *Advances in Neural Information Processing Systems*, 2022. 7
- Stewart Mayhew. Implied volatility. *Financial Analysts Journal*, 51(4):8–20, 1995. 18
- P Warwick Millar. Robust estimation via minimum distance methods. *Zeitschrift für Wahrscheinlichkeitstheorie und verwandte Gebiete*, 55(1):73–89, 1981. 2
- Peyman Mohajerin Esfahani and Daniel Kuhn. Data-driven distributionally robust optimization using the wasserstein metric: Performance guarantees and tractable reformulations. *Mathematical Programming*, 171(1):115–166, 2018. 7
- Chanseok Park, Ayanendranath Basu, and Srabashi Basu. Robust minimum distance inference based on combined distances. *Communications in Statistics-Simulation and Computation*, 24(3):653–673, 1995. 2
- William C Parr and William R Schucany. Minimum distance and robust estimation. *Journal of the American Statistical Association*, 75(371):616–624, 1980. 2
- Benjamin Peirce. Criterion for the rejection of doubtful observations. *The Astronomical Journal*, 2:161–163, 1852. 1
- Gabriel Peyré, Marco Cuturi, et al. Computational optimal transport: With applications to data science. *Foundations and Trends® in Machine Learning*, 11(5-6):355–607, 2019. 2, 5
- R Tyrrell Rockafellar and Roger J-B Wets. *Variational Analysis*, volume 317. Springer Science & Business Media, 2009. 10
- Peter J. Rousseeuw and Annick M. Leroy. *Robust regression and outlier detection*. Wiley Series in Probability and Mathematical Statistics: Applied Probability and Statistics. John Wiley & Sons, Inc., 1987. 2
- Mark Rubinstein. Implied binomial trees. *The Journal of Finance*, 49(3):771–818, 1994. 20
- Soroosh Shafieezadeh Abadeh, Peyman M Mohajerin Esfahani, and Daniel Kuhn. Distributionally robust logistic regression. In *Advances in Neural Information Processing Systems* 28, 2015. 2
- Soroosh Shafieezadeh-Abadeh, Daniel Kuhn, and Peyman Mohajerin Esfahani. Regularization via mass transportation. *Journal of Machine Learning Research*, 20(103):1–68, 2019. 2
- Aman Sinha, Hongseok Namkoong, and John Duchi. Certifying some distributional robustness with principled adversarial training. In *International Conference on Learning Representations*, 2018. 2
- Robin Thompson. A note on restricted maximum likelihood estimation with an alternative outlier model. *Journal of the Royal Statistical Society: Series B (Methodological)*, 47(1):53–55, 1985. 1
- John W Tukey. *Exploratory Data Analysis*. Addison-Wesley, 1977. 1
- John Wilder Tukey. A survey of sampling from contaminated distributions. *Contributions to probability and statistics*, pp. 448–485, 1960. 2

- Cédric Villani. *Optimal Transport: Old and New*, volume 338. Springer, 2009. 2, 5
- Wolfram Wiesemann, Daniel Kuhn, and Melvyn Sim. Distributionally robust convex optimization. *Operations Research*, 62(6):1358–1376, 2014. 2
- Man-Chung Yue, Daniel Kuhn, and Wolfram Wiesemann. On linear optimization over wasserstein balls. *Mathematical Programming*, 195(1-2):1107–1122, 2022. 9
- Luhao Zhang, Jincheng Yang, and Rui Gao. A simple and general duality proof for wasserstein distributionally robust optimization. *arXiv preprint arXiv:2205.00362*, 2022. 7
- Banghua Zhu, Jiantao Jiao, and Jacob Steinhardt. Generalized resilience and robust statistics. *The Annals of Statistics*, 50(4):2256–2283, 2022. 2



# Appendix

## A Organization of the Appendix

We organize the appendix as follows:

- The proof of Theorem 4.1 and Theorem 4.2 are given in Section B.1.
- The long haul structure for linear regression with a concave cost function is provided in Section B.2.
- Additional details on mean estimation simulations are given in Section C.1.
- Additional plots for the mean estimation simulations for the concave cost function are given in Section C.2.
- Additional plots for the mean estimation simulations for the convex cost function are given in Section C.3.
- Additional details on LAD regression simulations are given in Section C.4.
- Additional plots for the LAD regression simulations for the concave cost function are given in Section C.5.
- Additional plots for the LAD regression simulations for the convex cost function are given in Section C.6.
- Additional option volatility surface experiment details are given in Section C.7.
- Additional information on the volatility surface data set and losses are given in Section C.8.

## B Proof details

### B.1 The proof of Theorem 4.1 and Theorem 4.2.

To start with, we give two crucial lemmas B.1 and B.2.

**Lemma B.1.** Suppose that  $a, b, \lambda > 0$  and  $r \in (0, 1)$ , we have

$$\min_{x \in [0, a/b]} a - bx + \lambda x^r = \min \left\{ a, \frac{\lambda a^r}{b^r} \right\}.$$

□

*Proof.* The argument is easy. The function  $g(x) = a - bx + \lambda x^r$  is concave as the second derivative is always negative:

$$\nabla^2 g(x) = \lambda r(r-1)x^{r-2}$$

for all  $x \geq 0$ . ■

**Lemma B.2.** Suppose that there is an increasing sequence  $0 \leq x_1 < x_2 < \dots < x_n$ . The optimal solution of

$$\max_{\lambda \geq 0} \sum_{i=1}^n \alpha_i \min\{x_i, \lambda x_i^r\} - \lambda \delta$$

is  $\lambda^* = x_k^{1-r}$  where

$$k := \max_{k \in [n]} \left\{ k : \sum_{i=k}^n \alpha_i x_k^r \geq \delta \right\}.$$

Here  $\alpha_i \in [0, 1]$ ,  $\sum_{i=1}^n \alpha_i = 1$ ,  $\delta > 0$  and  $r \in (0, 1)$ . Moreover, the optimal function value is

$$\max \left( \sum_{i=1}^{k-1} \alpha_i x_i + \left( 1 - \frac{(\delta - \sum_{i=k+1}^n \alpha_i x_i^r)}{\alpha_k x_k^r} \right) \alpha_k x_k, 0 \right).$$

□

*Proof.* Without loss of generality, we assume that  $0 < x_1 < x_2 < \dots < x_n$  as the zero part of the sequence does not affect the result.

First, given a fixed  $\lambda \in \mathbb{R}_+$  and the inequality  $x_{t+1} < \lambda x_{t+1}^r$ , our goal is to show that  $x_t < \lambda x_t^r$ . Let  $x_t = \eta x_{t+1}$ , where  $\eta \in (0, 1]$ . Then, we have

$$x_t = \eta x_{t+1} < \eta \lambda x_{t+1}^r = \frac{\lambda}{\eta^r} \eta x_t^r = \lambda \eta^{1-r} x_t^r \leq \lambda x_t^r.$$

Considering a fixed  $\lambda \in \mathbb{R}_+$ , we can express the objective function as:

$$\sum_{i=1}^n \alpha_i \min\{x_i, \lambda x_i^r\} - \lambda \delta = \sum_{i=1}^{k-1} \alpha_i x_i + \alpha_k \min\{x_k, \lambda x_k^r\} + \lambda \sum_{i=k+1}^n \alpha_i x_i^r - \lambda \delta$$

where  $1 \leq k \leq n$  and  $\alpha_i$  are weights associated with each  $x_i$ . Two cases arise:

1. For all  $1 \leq t \leq k-1$ ,  $x_t < \lambda x_t^r$ , or for all  $k+1 \leq t \leq n$ ,  $x_t > \lambda x_t^r$ .
2. At the  $k$ -th point, we have  $x_k = \lambda x_k^r$ .

Since we are dealing with a concave piecewise linear function, the optimal  $\lambda$  will be a knot point (case 2). Otherwise, modifying  $\lambda$  would increase the objective value. Therefore, we can establish the first-order optimality condition as follows:

$$\sum_{i=k+1}^n \alpha_i x_i^r + \mu \alpha_k x_k^r = \delta.$$

where  $k$  and  $\mu \in [0, 1]$  are determined through a search using the quick-select algorithm. Consequently, the optimal solution is obtained as  $\lambda^* = x_k^{1-r}$  and

$$k = \max_{k \in [n]} \left\{ \sum_{i=k}^n \alpha_i x_i^r \geq \delta \right\}.$$

Thus, we further get  $\mu = \frac{(\delta - \sum_{i=k+1}^n \alpha_i x_i^r)}{\alpha_k x_k^r}$  and the optimal function value admits

$$\begin{aligned} & \sum_{i=1}^{k-1} \alpha_i x_i + \alpha_k \min\{x_k, \lambda x_k^r\} + \lambda \sum_{i=k+1}^n \alpha_i x_i^r - \lambda \delta \\ &= \sum_{i=1}^{k-1} \alpha_i x_i + \alpha_k \min\{x_k, \lambda x_k^r\} - \lambda \mu \alpha_k x_k^r \\ &= \sum_{i=1}^{k-1} \alpha_i x_i + (1 - \mu) \alpha_k x_k \\ &= \sum_{i=1}^{k-1} \alpha_i x_i + \left( 1 - \frac{(\delta - \sum_{i=k+1}^n \alpha_i x_i^r)}{\alpha_k x_k^r} \right) \alpha_k x_k \end{aligned}$$

Based on our discussion, we exclude the corner case where  $k = 1$ . Therefore,  $\delta$  is sufficiently large such that  $\sum_{i=1}^n \alpha_i x_i^r \leq \delta$ . It's evident that in this trivial scenario, the optimal function value is zero.

We conclude our proof. ■

## Proof of Theorem 4.2

### B.2 Linear Regression with Concave Cost Function

In this subsection, we aim to illustrate an example as mentioned in Section 4.2. Suppose we choose a concave cost function  $c$  that grows strictly slower than the loss function  $f$ . In such a scenario, when the budget is limited, the rectified data point  $z_{\text{best}}$  consistently demonstrates the long-haul structure, thereby ensuring automatic outlier identification properties.

**Example B.1.** Suppose that  $\mathcal{Z} = \mathbb{R}^{d+1}$ ,  $\ell(\theta, z) = \|y - \theta^T x\|^2$  and the cost function is defined as  $c(z, z') = \|z - z'\|^r$  where  $r = \frac{1}{2}$ . We want to study the best rectification distribution of

$$\min_{Q \in \mathcal{R}(\mathbb{P}'_n)} \mathbb{E}_Q[\|y - \theta^T x\|^2].$$

□

As we shall see when the dual variable  $\lambda$  is relatively small, the best rectification distribution will keep the long-haul structure although the inner minimization problem is no longer concave.

For simplicity, we denote  $\tilde{\theta} = (\theta, -1)$  and  $z = (x, y)$ . By the strong duality result in Proposition 4.1, we only have to focus on the inner minimization problem:

$$\begin{aligned} & \min_{\Delta \in \mathbb{R}^{d+1}} \left\{ (\tilde{\theta}^T (Z' + \Delta))^2 + \lambda \|\Delta\|^r \right\} \\ &= \min_{\|\Delta\| \leq \frac{|\tilde{\theta}^T Z'|}{\|\tilde{\theta}\|_*}} \left\{ (|\tilde{\theta}^T Z'| - \|\tilde{\theta}\|_* \|\Delta\|)^2 + \lambda \|\Delta\|^r \right\}. \end{aligned}$$

Next, we aim at clarifying the structured information of the following one-dimensional optimization problem:

$$\min_{\|\Delta\| \in \left[0, \frac{|\tilde{\theta}^T Z'|}{\|\tilde{\theta}\|_*}\right]} K(\|\Delta\|) := (|\tilde{\theta}^T Z'| - \|\tilde{\theta}\|_* \|\Delta\|)^2 + \lambda \|\Delta\|^r.$$

In general, unlike the case of absolute loss, the function  $K(\cdot)$  will not be concave. However, the optimal solution of the resulting optimization problem will be active at the boundary when  $\delta$  is small and the optimal value of  $\lambda$  is sufficiently large. Initially, let's overlook the constraint and express the first-order optimality condition.

$$\begin{aligned} & 2\|\tilde{\theta}\|_* (\|\tilde{\theta}\|_* \|\Delta\| - |\tilde{\theta}^T Z'|) + \frac{1}{2} \lambda \|\Delta\|^{-\frac{1}{2}} = 0 \\ \Rightarrow & \|\tilde{\theta}\|_*^2 \|\Delta\| + \frac{\lambda}{4} \|\Delta\|^{-\frac{1}{2}} = |\tilde{\theta}^T Z'| \|\tilde{\theta}\|_* \\ \Rightarrow & \|\tilde{\theta}\|_*^2 \|\Delta\|^{\frac{3}{2}} + \frac{\lambda}{4} = |\tilde{\theta}^T Z'| \|\tilde{\theta}\|_* \|\Delta\|^{\frac{1}{2}}. \end{aligned}$$

By changing the variable  $\beta = \|\Delta\|^{\frac{1}{2}}$ , we have

$$\|\tilde{\theta}\|_*^2 \beta^3 + \frac{\lambda}{4} - |\tilde{\theta}^T Z'| \|\tilde{\theta}\|_* \beta = 0.$$

Now, we observe that  $g(\beta) = \|\tilde{\theta}\|_*^2 \beta^3 + \frac{\lambda}{4} - |\tilde{\theta}^T Z'| \|\tilde{\theta}\|_* \beta$ , and our objective is to find the positive root of this cubic equation in one dimension. Also, the first derivative is  $\nabla g(\beta) = 3\|\tilde{\theta}\|_*^2 \beta^2 - |\tilde{\theta}^T Z'| \|\tilde{\theta}\|_*$ . The stationary point is  $\beta^* = \sqrt{\frac{|\tilde{\theta}^T Z'|}{3\|\tilde{\theta}\|_*}}$  and then the corresponding  $\|\Delta^*\| = \frac{|\tilde{\theta}^T Z'|}{3\|\tilde{\theta}\|_*} \in [0, \frac{|\tilde{\theta}^T Z'|}{\|\tilde{\theta}\|_*}]$ .

$$g(\beta^*) = \left( \sqrt{\frac{|\tilde{\theta}^T Z'|}{3\|\tilde{\theta}\|_*}} \right)^3 \|\tilde{\theta}\|_*^2 - |\tilde{\theta}^T Z'| \|\tilde{\theta}\|_* \sqrt{\frac{|\tilde{\theta}^T Z'|}{3\|\tilde{\theta}\|_*}} + \frac{\lambda}{4}.$$

1. When  $\lambda \geq 4 \left( |\tilde{\theta}^T Z'| \|\tilde{\theta}\|_* \sqrt{\frac{|\tilde{\theta}^T Z'|}{3\|\tilde{\theta}\|_*}} - \left( \sqrt{\frac{|\tilde{\theta}^T Z'|}{3\|\tilde{\theta}\|_*}} \right)^3 \right)$  (i.e.,  $\delta$  is sufficiently small), we have  $g(\beta^*) \geq 0$ .

As such, the critical point of the unconstrained optimization problem is not in the interval  $[0, \frac{|\tilde{\theta}^T Z'|}{\|\tilde{\theta}\|_*}]$ . In other words, we can conclude the optimal solution will be 0 and the solution of vanilla least square is already optimal.

2. When  $g(\beta^*) < 0$ , we know there are two solutions  $\beta_+, \beta_-$  for  $g(\beta) = 0$  where  $\beta_- < \beta_+$ . We know  $K(\|\Delta\|)$  will be increasing between  $[0, \beta_-^2]$  and decreasing between  $[\beta_-^2, \beta_+^2]$ . Thus, the optimal solution will be either 0 or  $\beta_+^2$  and ensures the long haul transportation structure. Different from the absolute loss, the cost function  $\|z - z'\|^{1/2}$  is not powerful enough to move any points that achieve a perfect fit to the current hyperplane.

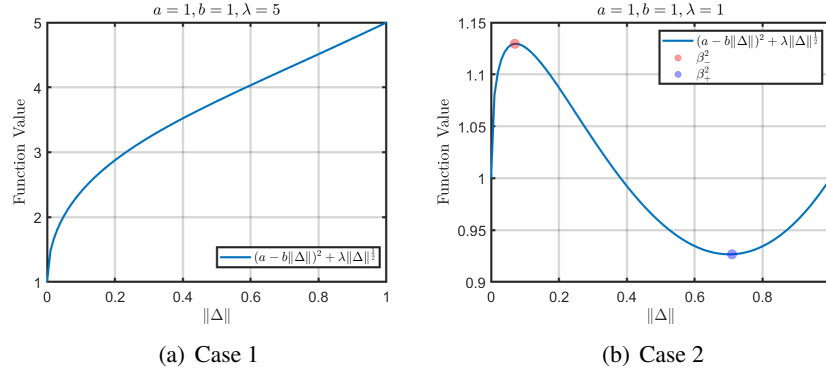


Figure 6: Visualization

## C Additional Experiments & Experimental Details

### C.1 Mean Estimation Details

The experimental details for mean estimation follow. For each  $(\delta, r)$  point in our experiments, we perform 100 random trials at 100 fixed seeds. In each trial, we run our optimization procedure for with a learning rate of  $10^{-2}$ . We stop when the number of iterations reaches 2000 or the change in the loss function between successive iterations is below a tolerance of  $10^{-6}$ . We initialize  $\theta$  to the median of the data set.

Below in Figure 7, we visualize the sensitivity analysis of  $r$  at  $\delta = 1$  when the corruption level is 45%. As shown, our concave transport cost function improves significantly on the linear cost function ( $r = 1$ ) and has a wide region of favorable stable performance.

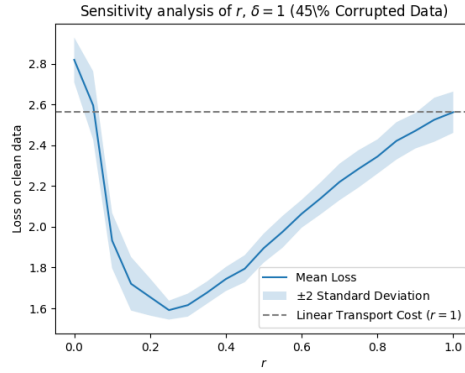


Figure 7: The sensitivity analysis of the loss on clean data with respect to  $r$  of our estimator at  $\delta = 1$  on data with a 45% corruption level on the mean estimation task.

## C.2 Concave Cost Mean Estimation Simulation

In Figure 8 below, we plot the evolution of the rectified distribution produced by our estimator under various values of  $\delta$  for the **concave** cost function with  $r = 0.5$ .

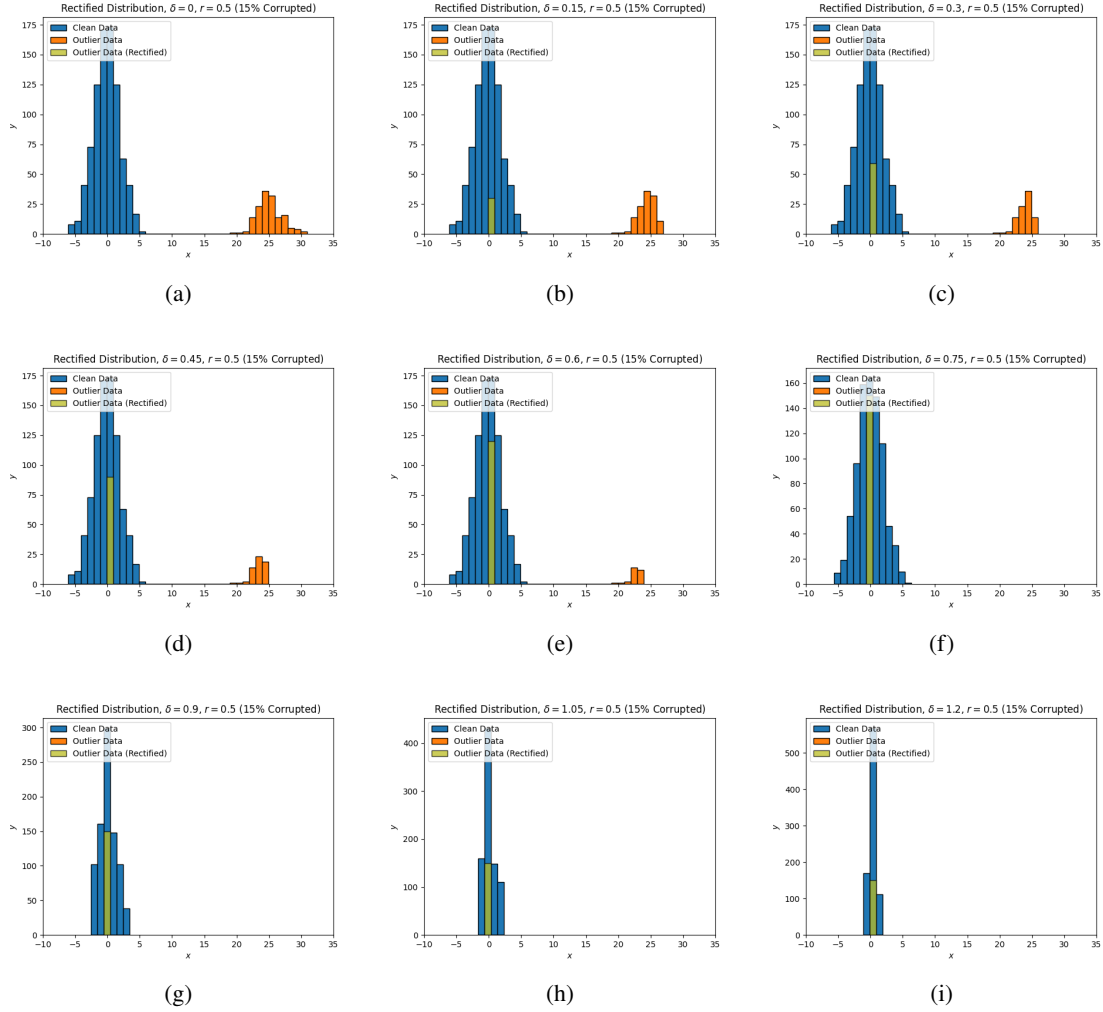


Figure 8: Visualization of the evolution of the rectified distribution.



### C.3 Convex Cost Mean Estimation Simulation

In the Figure 9 below, we plot the evolution of the rectified distribution produced by our estimator under various values of  $\delta$  for the **convex** cost function with  $r = 2.0$ .

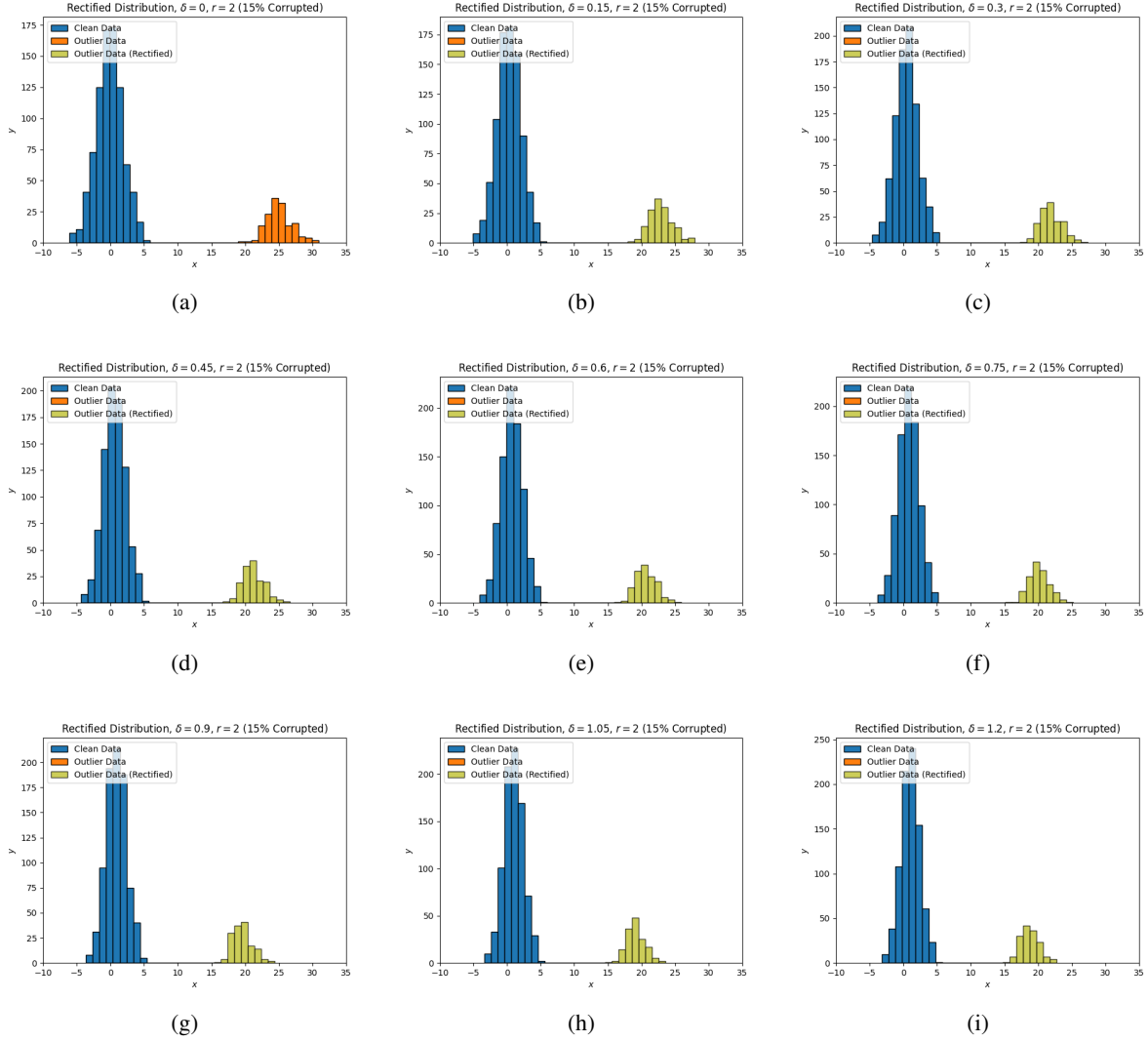


Figure 9: Visualization of the evolution of the rectified distribution.

## C.4 Least Absolute Regression Details

The experimental details for least absolute regression follow. For each  $(\delta, r)$  point in our experiments, we perform 100 random trials at 100 fixed seeds. In each trial, we run our optimization procedure for with a learning rate of  $10^{-2}$  starting from 10 randomly initialized points and take the best loss. In each problem, we stop optimization when the number of iterations reaches 1000 or the change in the loss function between successive iterations is below a tolerance of  $10^{-6}$ . We initialize the slope  $\beta$  according to a  $N(0, 1)$  distribution and the bias to zero.

We provide additional results on the least absolute deviation simulations below. In Table 4 we report the results of our experiment. We also test our cross-validation procedure in the LAD regression context to show that it improves the selection of the budget  $\delta$ . We take the same experimental setting as in the regression example from the main text. In particular, our algorithm for cross-validation which proceeds as follows:

1. First, we draw a small sample of size  $N = 8$  from the dataset. If a corruption level is suspected, it may be used to find a reasonable sample size for this purpose using a binomial probability calculation. We have tried several small values from  $N = 5$  to  $N = 10$  and found the performance to be relatively similar.
2. Using this sample, we fit our robust estimator for a range of values of  $\delta$ , the budget parameter. We use  $\delta \in \{0.5, 1.0, 1.5, 2.0, 2.5, 3.0\}$ . We select the  $\delta$  which produces the smallest loss on this sample data set.
3. Using the optimal  $\delta$  selected in step 2, we fit our robust estimator on the entire dataset. The results of this procedure are displayed in Table 4.

The results are included in Table 4. As can be seen, our estimator outperforms all competing estimators, and attains significant outperformance for most corruption levels. Cross-validation significantly improves the results for several settings of  $\epsilon$ , but performs worse than our fixed  $\delta$  for some of the larger values of  $\epsilon$ . We hypothesize that this is due to the impossibility of distinguishing which distribution is the “correct” distribution as  $\epsilon \rightarrow 0.5$ , which may lead to learning regression slopes which fit the corruption distribution instead of the clean distribution. However, for smaller values of  $\epsilon$ , we see a moderate improvement due to cross-validation.

In Figure 10 and Figure 11 below, we plot the sensitivity of our estimator across different values of  $\delta$  and  $r$ . We see that there is a reasonable basin of good performance across both values. Each loss curve approaches the error of benchmark estimator or estimator with a traditional cost function as we let  $\delta$  and  $r$  tend toward values which recover these approaches.

Corruption Level	20%	30%	40%	45%	49%
OLS	$1.569 \pm 0.041$	$1.702 \pm 0.043$	$1.773 \pm 0.049$	$1.803 \pm 0.052$	$1.822 \pm 0.054$
LAD	$1.808 \pm 0.131$	$1.875 \pm 0.055$	$1.892 \pm 0.059$	$1.903 \pm 0.061$	$1.908 \pm 0.062$
Huber	$1.642 \pm 0.042$	$1.776 \pm 0.045$	$1.842 \pm 0.053$	$1.868 \pm 0.056$	$1.882 \pm 0.059$
Ours	<b><math>0.803 \pm 0.860</math></b>	<b><math>0.574 \pm 0.778</math></b>	<b><math>0.355 \pm 0.878</math></b>	<b><math>0.462 \pm 0.962</math></b>	<b><math>0.572 \pm 0.998</math></b>
Ours (CV)	<b><math>0.349 \pm 0.784</math></b>	<b><math>0.509 \pm 0.898</math></b>	<b><math>0.667 \pm 1.184</math></b>	<b><math>0.832 \pm 1.354</math></b>	<b><math>0.750 \pm 1.282</math></b>

Table 4: We compared our estimator with several standard regression methods by evaluating the average loss on clean data points across various corruption levels. Mean performance is accompanied by a 95% confidence interval over 100 random trials. In our evaluation, we set the threshold parameter of Huber regression to 1.5. The hyperparameters for our estimator, namely  $\delta = 1.5$  and  $r = 0.5$ , remained constant across all corrupted levels.

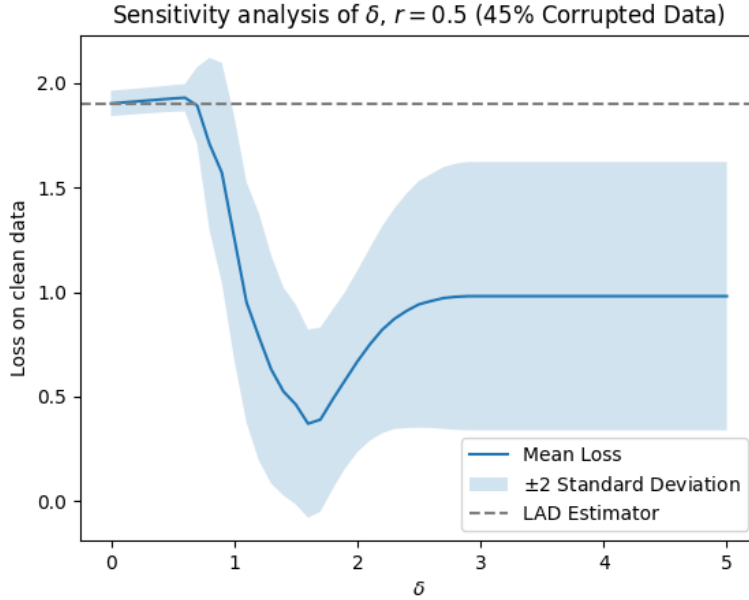


Figure 10: The sensitivity analysis of the loss on clean data with respect to  $\delta$  of our estimator at  $r = 0.5$  on data with a 45% corruption level on the least absolute regression task.

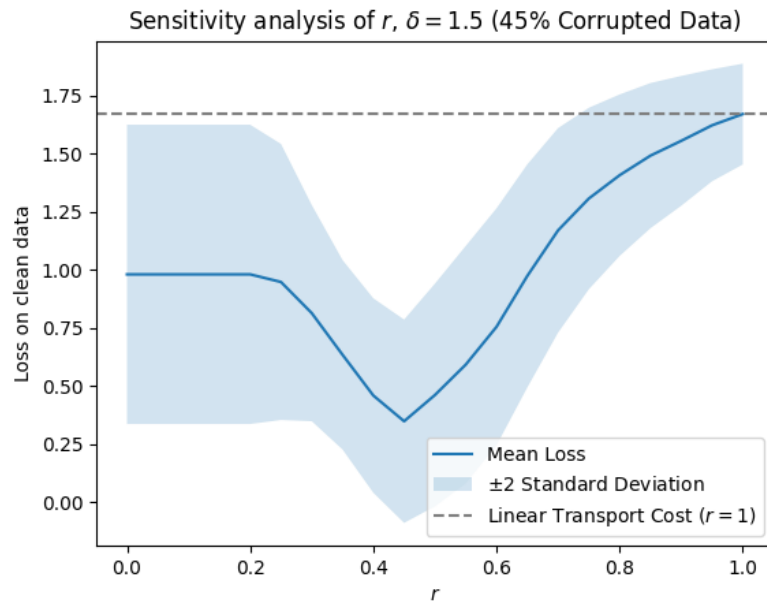


Figure 11: The sensitivity analysis of the loss on clean data with respect to  $r$  of our estimator at  $\delta = 1.5$  on data with a 45% corruption level on the least absolute regression task.

## C.5 Concave Cost Regression Simulation

In the Figure 12, we plot the evolution of the rectified distribution and line of best fit produced by our LAD regression estimator under various values of  $\delta$  for the **concave** cost function with  $r = 0.5$ .

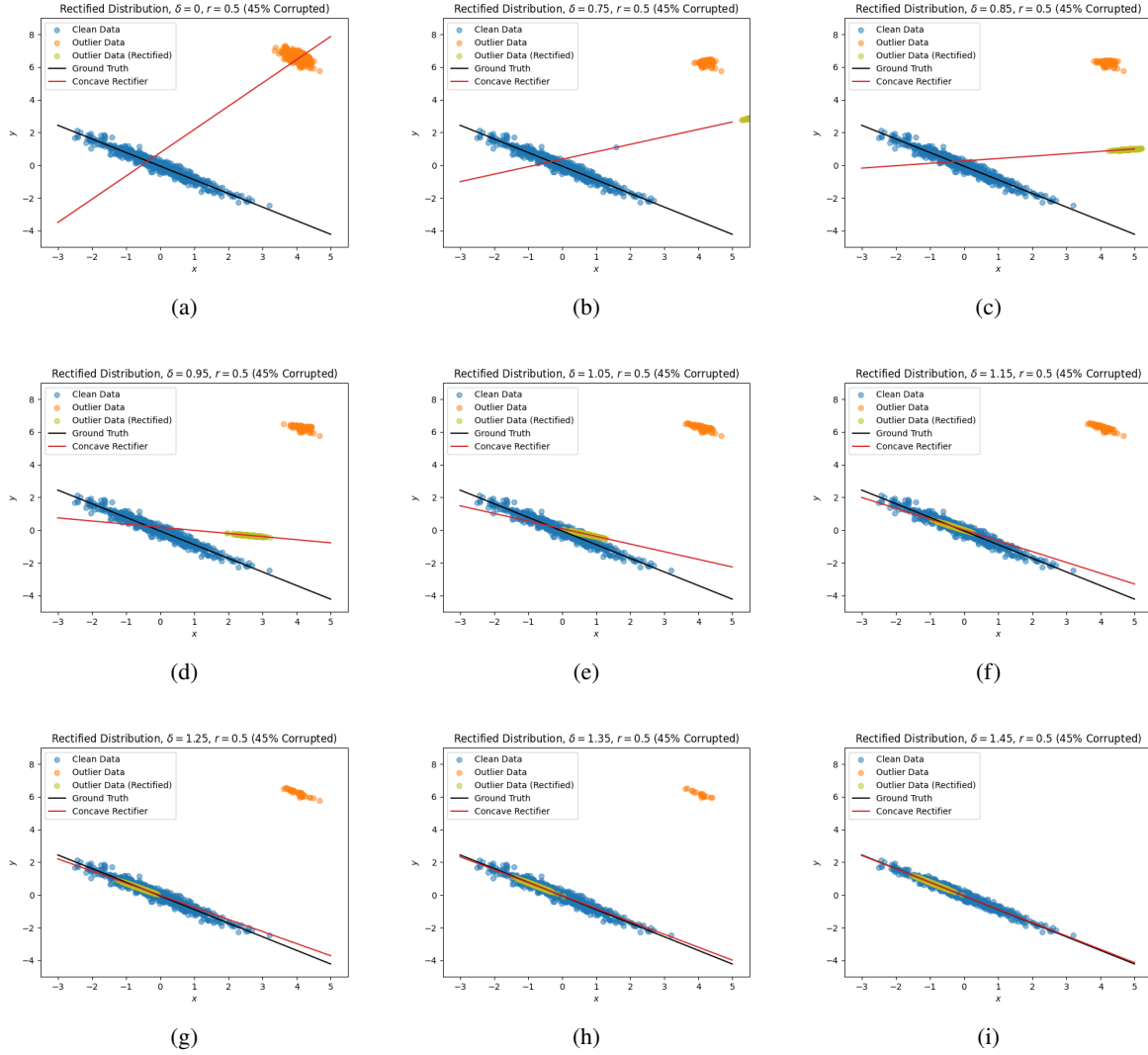


Figure 12: Visualization of the evolution of the rectified distribution.

## C.6 Convex Cost Regression Simulation

In the Figure 13, we plot the evolution of the rectified distribution and line of best fit produced by our LAD regression estimator under various values of  $\delta$  for the **convex** cost function with  $r = 2.0$ .

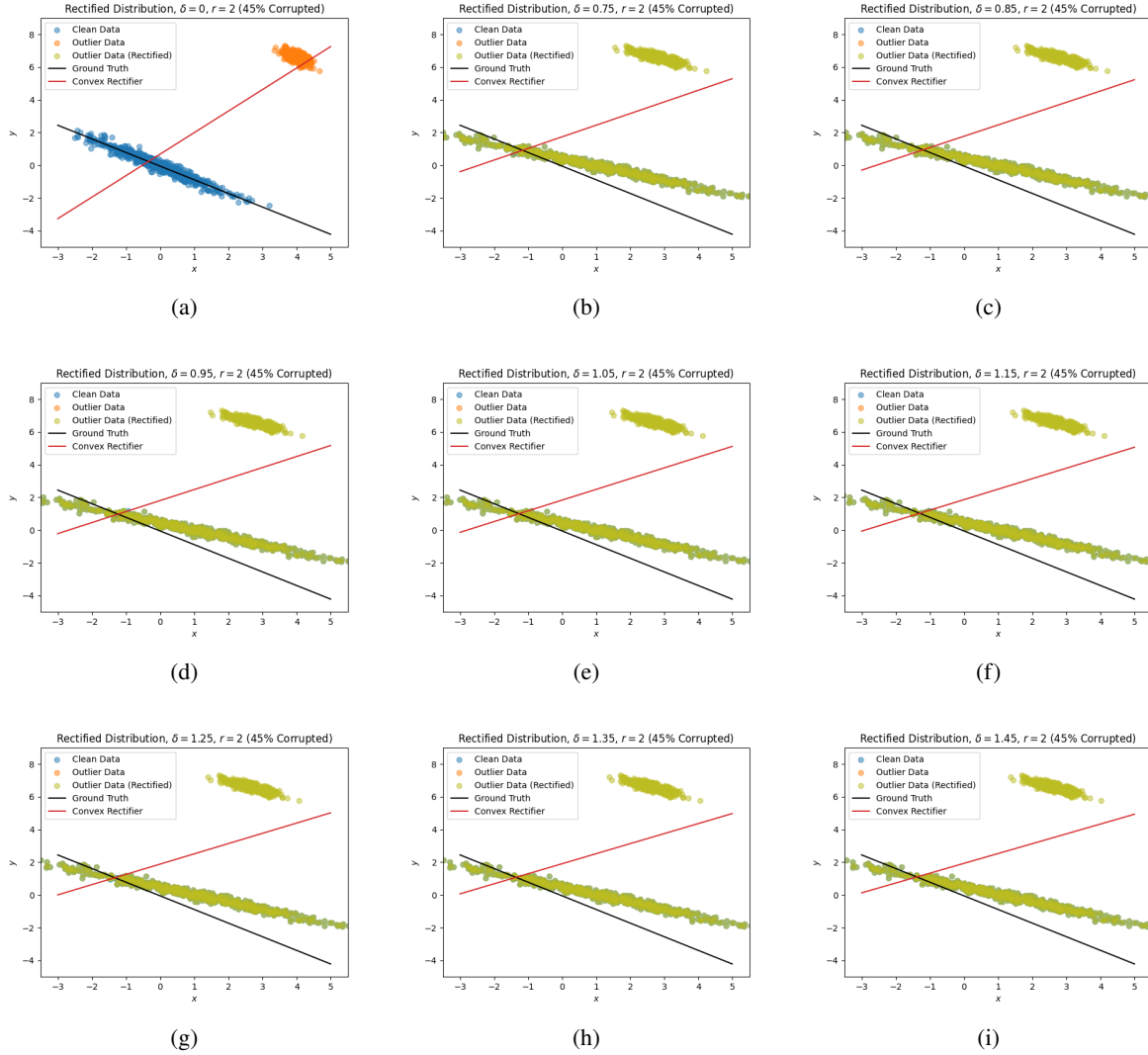


Figure 13: Visualization of the evolution of the rectified distribution.

## C.7 Additional Volatility Surface Experiment

We have performed an additional experiment to demonstrate the practicality of our method and the selection of the parameter  $\delta$  with the realistic options outlier data set of our empirical study. This experiment shows that our method leads to better out-of-sample results on complex data and does not require the availability of clean data. The problem is the estimation of the volatility surface in the presence of outliers for the option data.

Our experiment proceeds as follows. In this experiment, the data set is organized as a list of (train day, test day) tuples. Train and test days are consecutive days for the same underlying security. On the train day, we estimate our model with different methods. On the consecutive trading day (that is, the test day) we use the estimated model to obtain out-of-sample evaluation metrics for the surface (MAPE and  $\nabla \hat{S}$ ). Note that this approach follows closely how volatility surfaces are used in practice by traders. This allows us to obtain the out-of-sample MAPE and  $\nabla \hat{S}$  as a function of  $\delta$ . The prior Appendix section provides the details of our empirical setup.

Our cross-validation procedure splits the train day into a training and validation sample, which we use to obtain estimates of MAPE and  $\nabla \hat{S}$  as a function of  $\delta$ . We select the delta that optimizes MAPE and  $\nabla \hat{S}$  and fit on the entire train day. Then, on the out-of-sample test day, we evaluate our method for the optimally selected  $\delta$ . Thus, to be clear, for the estimated optimal  $\delta$ , we estimate the surface on one day, and evaluate it completely out-of-sample on the consecutive trading day.

The results are collected in the table below. The results of our experiment show that our cross-validation approach outperforms competing approaches and improves upon the fixed  $\delta$  results reported in the main text. The below tables show the out-of-sample MAPE and  $\nabla \hat{S}$  averaged over all out-of-sample test days.

Model MAPE	0.5% Quantile	5% Quantile	Median	Mean	95% Quantile	99.5% Quantile
KS	0.047	0.088	0.236	0.274	0.563	1.033
2SKS	0.036	0.065	0.172	0.216	0.504	0.999
Ours ( $\delta = 10^{-2}$ )	0.037	0.065	0.170	0.203	0.440	0.841
Ours (CV)	0.036	0.064	0.170	0.203	0.437	0.837
Model $\nabla \hat{S}$	0.5% Quantile	5% Quantile	Median	Mean	95% Quantile	99.5% Quantile
KS	0.323	1.616	14.042	19.653	59.534	105.361
2SKS	0.036	0.121	1.759	6.823	30.020	76.652
Ours ( $\delta = 10^{-2}$ )	0.035	0.112	1.579	5.880	25.521	70.708
Ours (CV)	0.033	0.104	1.248	4.522	19.645	55.261

Table 5: Median and quantiles of the distribution of MAPE or  $\nabla \hat{S}$  across all samples for KS, 2SKS, and our methods. Our estimator achieves significantly lower MAPE and  $\nabla \hat{S}$  than the benchmark KS estimator and improves upon the 2SKS estimator. Our CV procedure improves even further.



## C.8 Options Volatility Surface Details

**Data set.** Our data set is derived from European-style US equity options implied volatilities from the years 2019–2021. The data come from the OptionMetrics IvyDB US database accessed through Wharton Research Data Services (WRDS). Implied volatilities created by OptionMetrics are calculated using the Black-Scholes formula using interest rates derived from ICE IBA LIBOR rates and settlement prices of CME Eurodollar futures. Option prices are set to the midpoint of the best bid and offer quoted for the option captured at 3:59 PM ET.

We developed our options surface estimator code in partnership with a major global provider of financial data, indices, and analytical products. This provider had previously identified 1,970 outlier-containing option chains for which they found IVS estimation challenging. These outlier-containing option chains were selected from all listed US equities on days within 2019–2021, and they comprise the data set used in our experiments. Because the code is proprietary, and the data set is a proprietary selection of surfaces, we cannot publicly release them. However, the data can be found in WRDS, and we provide all implementation details in this appendix section.

**Implementation.** We implement the KS estimator and our estimator in PyTorch. For our estimator, we estimate the surface by subgradient descent with learning rate  $\alpha = 10^{-1}$  and  $r = 0.5$ , terminating when the relative change in loss reaches  $10^{-5}$ . We denote the test data set’s option’s implied volatilities  $y'_i$  and the estimated surface’s implied volatility for option  $i$  as  $\hat{S}(x'_i)$ . We begin each iteration by setting  $\delta = \ell(x, y)/2\|\theta\|^r$ , where  $\ell$  is the loss function of Theorem 4.2. We initialize  $\theta$  to those of the benchmark estimator. We perform 5 trials per options chain. In each trial, we randomly select a different 80% train and 20% test set, estimate the surface on the train set, and record the two losses (MAPE and  $\nabla\hat{S}$ ) on the test set. We depict all losses gathered in this way via the histograms of Section 6. Experiments are run on a server with a Xeon E5-2398 v3 processor and 756GB of RAM.

**Cross-validation.** The cross-validation (CV) procedure samples 2/3 of the training surface as a CV training set and leaves the remaining 1/3 as the CV validation set. Empirically, we expect  $\epsilon$  to be quite small (e.g.  $\epsilon \in (0, 0.05]$ ) for this data set, which allows us to take a larger cross-validation set, as most option chains contain only a few hundred options. Five such random splits are drawn and used to estimate the MAPE of  $\delta \in \{10^{-6}, 10^{-5}, 10^{-4}, 10^{-3}, 10^{-2}, 10^{-1}, 1, 2, 5, 10\}$ . The MAPEs of each  $\delta$  are averaged across the five CV runs and the  $\delta$  with the lowest MAPE is then used to fit our estimator on the entire option chain.

**Losses.** We define the option implied volatility surface  $\hat{S}(x)$  as the function from *option feature vectors*  $x$  to *estimated implied volatilities*  $y$ . That is, for some given  $x$ , we have  $y := \hat{S}(x)$ . The accuracy measure MAPE is defined as follows for some test set of options  $\{(x'_i, y'_i)\}_{i=1}^n$ :

$$l_{\text{MAPE}}(\hat{S}, \{y'_i\}_{i=1}^n) = \frac{1}{n} \sum_{i=1}^n \frac{|\hat{S}(x'_i) - y'_i|}{|y'_i| + c}$$

where  $c$  is a small numerical stability factor we set to 0.01. This is a suitable choice, as  $\geq 99\%$  of implied volatilities are greater than 0.1.

The smoothness measure  $\nabla\hat{S}$  is defined as follows:

$$\nabla\hat{S} = \sum_{i=0}^{p-1} \sum_{j=0}^{s-1} \frac{(\hat{S}_{\tau_{i+1}, \Delta_j} - \hat{S}_{\tau_i, \Delta_j})^2 + (\hat{S}_{\tau_i, \Delta_{j+1}} - \hat{S}_{\tau_i, \Delta_j})^2}{2}$$

In the expression above,  $\hat{S}_{\tau_i, \Delta_j} := \hat{S}(\log \tau_i, u(\Delta_j), z)$  where  $z = 1$  if  $\Delta_j > 0$  and 0 otherwise. Here, each tuple  $(\tau_i, \Delta_j)$  is a member of the Cartesian product of  $\{\tau_j : j \in [p]\}$  and  $\{\Delta_k : k \in [s]\}$ , where "[ $m$ ]" denotes the set of natural numbers from 0 to  $m$ , and  $p = 10$  and  $s = 39$ . By convention, OptionMetrics selects the following 11 discretization points for  $\tau$ , which we follow:

$$\tau \in \{10, 30, 60, 91, 122, 152, 182, 273, 365, 547, 730\}.$$

For  $\Delta$ , we use the following 40 points, which are a superset of the set of discretization points which OptionMetrics selects:

$$\Delta \in \{-1.0 + 0.05m : m \in [40]\} \setminus \{0\}.$$

**Example implied volatility surfaces.** In the following surface figures, we display the significant outlier rectification effect of our estimator on a sample option chain which contains outliers. These examples serves to illustrate the efficacy of the automatic outlier rectification mechanism and to provide intuition for the surface fitting problem.

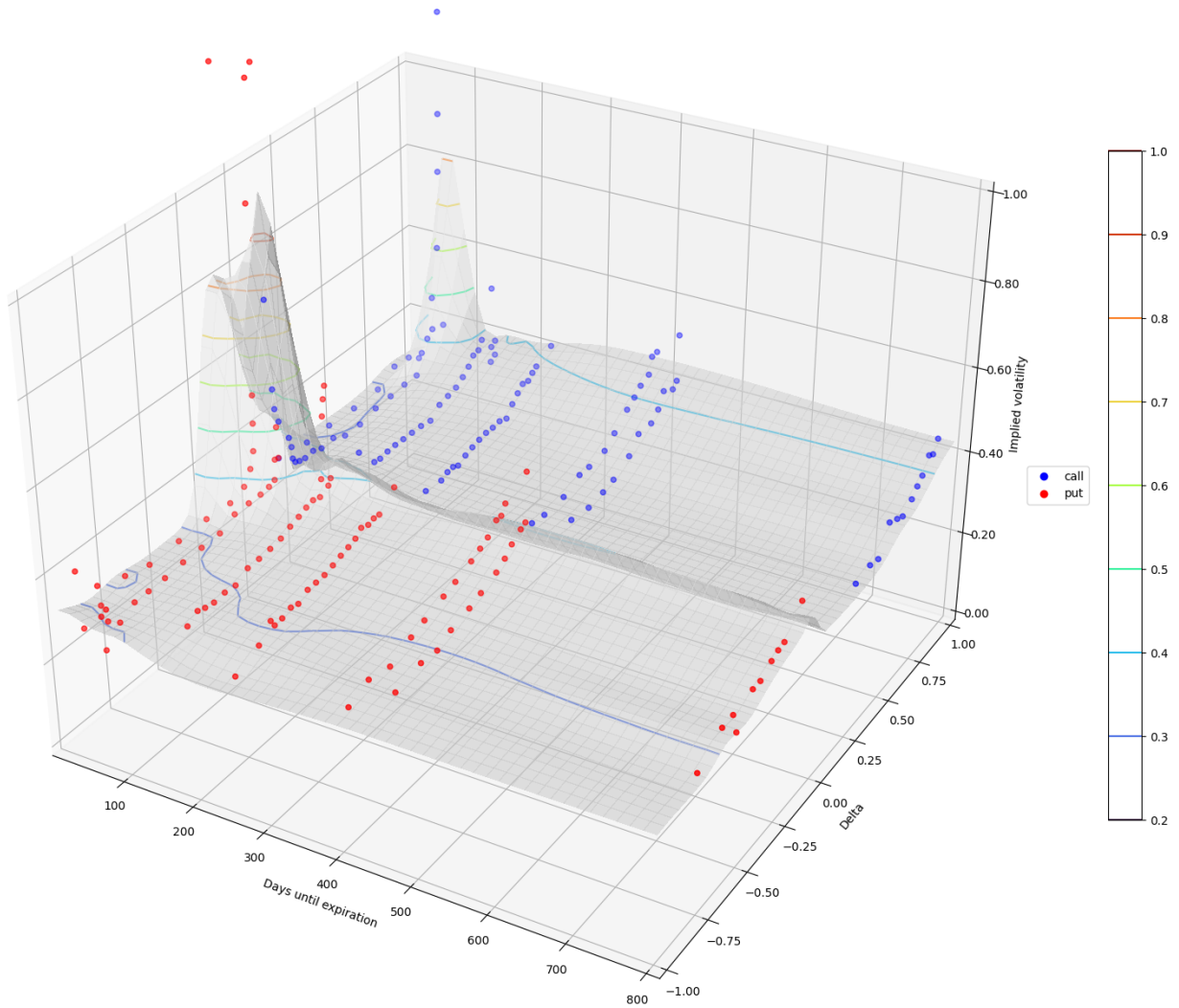


Figure 14: This plot depicts the option implied volatility surface estimated by the benchmark KS method on the options, which are depicted as blue and red dots. Blue denotes call options and red denotes put options. Outliers are present in this option chain near 0-100 days until expiration for deltas around  $\Delta = -0.2$  (approximately four put option outliers and 1 call option outlier) and  $\Delta = 1.0$  (approximately 3 call option outliers). These outliers heavily corrupt the fitted surface, wildly distorting the values around these deltas and causing a poor fit for surrounding options which are not outliers. The surface reaches values of 90% annualized implied volatility and has a surface gradient  $\nabla \hat{S}$  of 1.48.

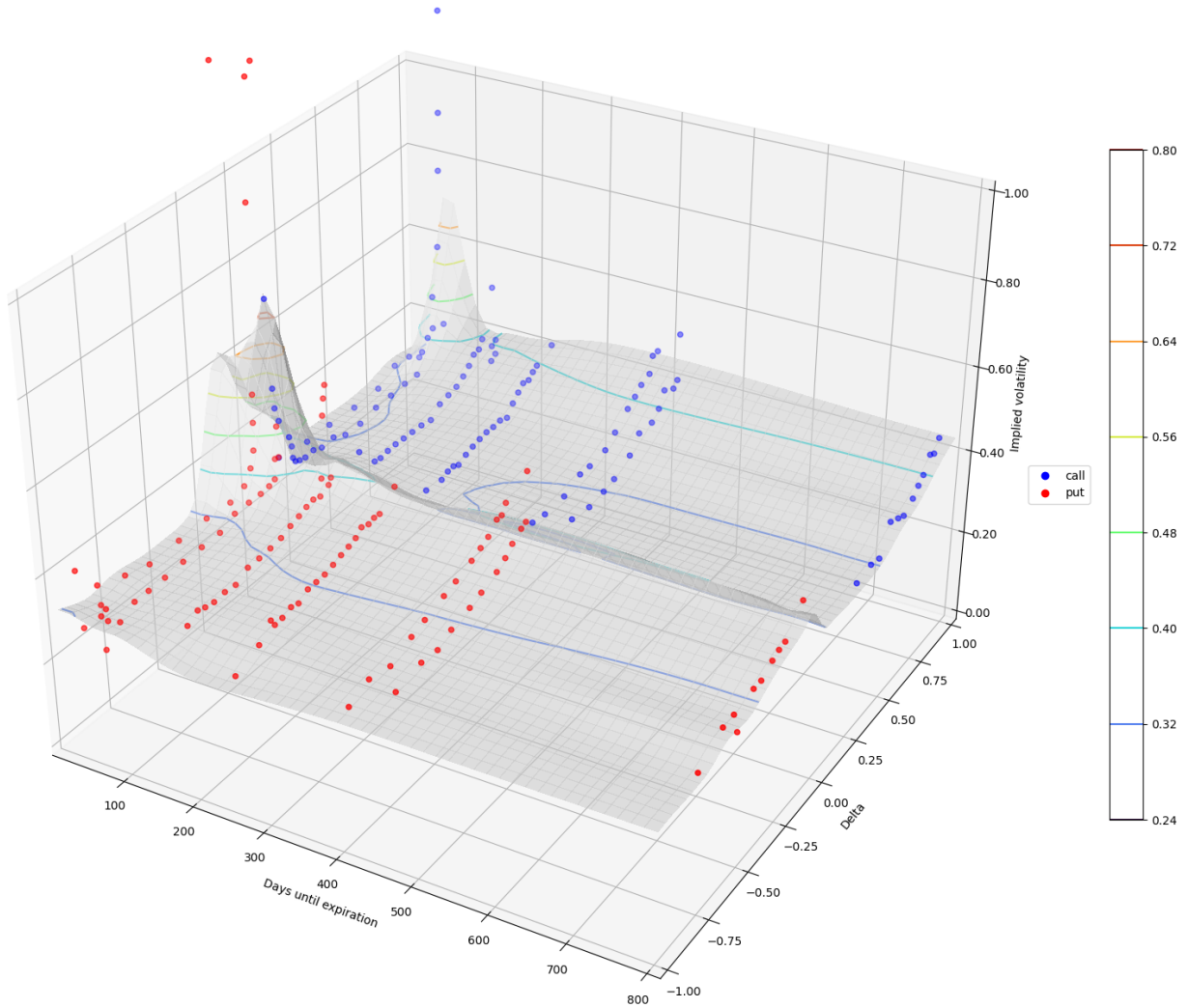


Figure 15: This plot depicts the option implied volatility surface  $\hat{S}(x)$  estimated by our estimator with  $\delta = 1$  on the displayed options, which are depicted as blue and red dots. Blue denotes call options and red denotes put options. Outliers are present in this option chain near 0-100 days until expiration for deltas around -0.2 and 1.0. However, these outliers do not corrupt the fitted surface, which fits options nearby the outlying options quite well as compared to the surface fit by the benchmark method displayed in the figure above. Additionally, in contrast to the surface fit by the benchmark KS method, the surface fit by our estimator only reaches values of  $\sim 65\%$  annualized implied volatility and has a surface gradient  $\nabla \hat{S}$  of 0.69, a smoothness improvement of over 100%. This example illustrates the capability of our estimator to rectify outliers.